Journal of Materials Chemistry A

Polyanionic insertion hosts for aqueous rechargeable batteries

Journal:	*Journal of Materials Chemistry A*
Manuscript ID	TA-REV-12-2021-011080.R1
Article Type:	Review Article
Date Submitted by the Author:	11-Feb-2022
Complete List of Authors:	Sharma, Lalit; The University of Texas at Austin Manthiram, Arumugam; The University of Texas at Austin, Materials Science and Engineering

REVIEW

Polyanionic insertion hosts for aqueous rechargeable batteries

Lalit Sharma[a] and Arumugam Manthiram[a,*]

Received 00th January 20xx,
Accepted 00th January 20xx

DOI: 10.1039/x0xx00000x

Safety concerns and costs of present-day lithium-ion batteries (LIBs) are prompting the development of alternate battery technologies with different types of electrolytes (*e.g.,* solid-state, gel-polymer, aqueous, *etc.*); notably, systems based on aqueous electrolytes have emerged as a promising alternative, especially for grid storage applications. The last decade has witnessed a considerable spike in the research carried out on aqueous batteries. However, the narrow operating voltage window of aqueous electrolytes and the structural instability of materials in aqueous media demand a proper selection of cathode materials to achieve desirable energy density. Polyanionic materials can be an ideal choice as they are structurally more stable and exhibit tunable redox potentials. This class of materials is considered as a storehouse in which many materials can be realized by substituting different polyanionic subunits. This review highlights some of the recent advances made in the polyanionic class of cathode materials for rechargeable aqueous batteries (Li-, Na- and Zn-ion batteries). The challenges facing the field, possible remedies to overcome them and future perspectives are also presented.

1. Introduction

The massive surge in energy demand of the growing population and dependence on non-renewable energy sources have led to critical environmental issues, especially greenhouse gas emissions. The transition from non-renewable to renewable energy sources, such as wind, tidal, hydro, and solar energies, requires efficient energy storage devices due to their intermittent nature. Hence, to enable renewable energy sources to supplant fossil fuels, developing safe and high energy density based rechargeable batteries is of the utmost importance. In this pursuit, lithium-ion batteries (LIBs) have dominated portable electronic devices and electric vehicles.[1–3] High cost and limited global lithium reserves have further led to the development of several alternative battery chemistries, such as sodium-ion and potassium-ion batteries involving, respectively, monovalent Na^+ and K^+ cations, as well as magnesium-ion, aluminum-ion, and zinc-ion batteries with, respectively, multivalent Mg^{2+}, Al^{3+}, and Zn^{2+} cations.[4–8] A brief comparison of the physical and electrochemical properties of these working ions is summarized in Table 1. Among all the chemistries mentioned above, sodium-ion batteries (SIBs) have shown tremendous potential to replace the existing LIBs for grid storage. Sodium is uniformly distributed in the earth's crust; hence, it is economical. Of late, the research on multivalent ion batteries has also intensified due to their high specific capacity and energy density, owing to the involvement of multiple electrons per ion in the redox reactions. However, there still exist roadblocks in developing safe electrolytes and finding suitable insertion-host materials.

The commercial lithium-ion batteries consist of oxide cathodes originated from Goodenough's group (*e.g.*, $LiCoO_2$ *etc.*), owing to their high specific capacity. However, these materials consist of expensive elements like cobalt. In this pursuit, various other materials have been investigated in past three decades, especially polyanionic class of materials.[9] The presence of a polyanionic subunit imparts thermal and structural stability as the oxygen atom is tightly bound to the central ion (P, S, Si, B, *etc.*). Hence, they are safer compared to oxide cathodes.[10] However, the specific capacity of polyanionic materials is low compared to oxides due to the presence of electrochemically inactive and bulky polyanionic subunits (PO_4^{3-}, BO_3^{3-}, SO_4^{2-} etc.). Yet, the inductive effect of the central metal ion of the polyanionic subunit increases the ionic character of the M-O bonds (M = Fe, Co, Ni *etc.*) and hence results in an increase in the redox potential. Therefore, the energy densities of polyanionic materials are increased, approaching that of oxide cathodes.

Apart from cost, safety is another major challenge for the existing battery technologies as the organic electrolytes used are flammable and toxic. The flammable nature of organic electrolytes coupled with the thermal runaway caused by electrode-electrolyte reactions poses a significant safety concern for the batteries.[11] Moreover, the assembly of batteries based on organic electrolytes requires strict oxygen and humidity-controlled chamber to avoid oxidation of the anode and avoid impurities in the electrolyte, which in turn adds up to the cost. These issues have intensified research in

[a] *Materials Science and Engineering Program & Texas Materials Institute, The University of Texas at Austin, Austin, TX, 75712 USA.*
*Corresponding Author. E-mail: manth@austin.utexas.edu.
Tel: +1-512-471-1791; Fax: +1-512-471-7681.

Table 1. Comparison of the physical and electrochemical properties of various working ions for aqueous batteries.

Working ion	Ionic radii (Å)	Electrode potential *vs.* SHE (V)	Specific gravimetric capacity (mA h g^{-1})	Specific volumetric capacity (mA h cm^{-3})
Li^+	0.76	-3.04	3862	2066
Na^+	1.02	-2.71	1166	1129
K^+	1.38	-2.93	685	586
Mg^{2+}	0.72	-2.37	2205	3832
Zn^{2+}	0.74	-0.76	820	5855
Al^{3+}	0.535	-1.66	2980	8046

finding a more suitable electrolyte, and different types of electrolytes have been reported.[12]

A possible way to circumvent the safety issue of organic electrolytes is the use of aqueous electrolytes.[11] Aqueous electrolytes not only impart inherent safety to the battery system but also are environmentally benign and offer two orders of magnitude higher ionic conductivity as compared to non-aqueous electrolytes, resulting in an enhanced round-trip efficiency. The use of these electrolytes does not demand any special environmental conditions, making aqueous batteries less expensive than non-aqueous batteries. Aqueous electrolytes have also seen applications in hybrid/aqueous metal-air batteries (Li or Na), which have emerged as an attractive energy storage systems owing to their high theoretical energy densities (3500 - 3800 W h kg^{-1}).[13–17] The discharge products in hybrid air batteries are soluble in the aqueous electrolyte and hence assists in better cycling performance and lower overpotential. Some of the major milestones in the field of aqueous batteries are shown in Fig. 1a. The concept of aqueous LIBs (ALIB) was first introduced by Dahn *et al.* in 1994 using a $LiMn_2O_4$ cathode and a β-VO_2 anode.[18] With 5 M $LiNO_3$ as an aqueous electrolyte, they obtained an average operating voltage of 1.5 V and an energy density of 55 W h kg^{-1}, much higher than that of lead-acid batteries (30 W h kg^{-1}). Since then, the field has witnessed a significant research being carried out on monovalent-ion (Li^+ and Na^+) and multivalent ion (Zn^{2+}, Mg^{2+}, and Al^{3+}) aqueous batteries.[19–25] Moreover, the development of "*water-in-salt*" (WISE) and "*water-in-bisalt*" (WIBSE) high concentrated electrolytes in 2015 have further addressed some of the critical problems like material dissolution, low operating voltage window etc., further revolutionizing the field of aqueous batteries as indicated by the increase in the number of research articles published on aqueous metal-ion batteries each year since 2015 (Fig. 1b).[26–28] Polyanionic cathode materials have been explored in detail with organic electrolytes for Li, Na, and Zn insertion. The tunable redox potentials of polyanionic cathodes have made them attractive candidates for aqueous batteries as well, and several reports in the literature.[29] Compared to oxide cathodes, polyanions are much more structurally stable in water due to their robust framework. This review displays some recent developments in polyanionic materials for aqueous rechargeable batteries, specifically Li-, Na-, and Zn- ion batteries. It will briefly discuss the challenges that existing polyanionic cathode materials face and strategies to overcome them, along with possible future directions.

2. Origin of polyanionic cathode materials

A typical lithium-ion battery consists of three major components, *i.e.*, a cathode and an anode separated by an electrolyte. During charge, lithium is extracted from the cathode and is inserted into the anode, while the opposite happens during discharge. Since lithium inventory originates from cathode, it limits the energy density of the battery. Schauffautl first showed the concept of intercalation in 1841 when he demonstrated intercalation of sulfate ions into graphite. Later, Whittingham reported chemical intercalation reactions in metal disulfides and reported the first rechargeable lithium battery at Exxon Corporation with TiS_2 cathode and lithium-metal anode.[30] However, the cell voltage was < 2.5 V, which limited the energy density and dendrite growth on lithium metal posed safety hazards. In order to enhance the cell voltage, Goodenough's group started exploring oxides in the 1980s. To have a high cell voltage, the redox energy of cathode should lie as low as possible and redox energy of anode should be as high as possible.[31] Utilizing the fundamental understanding of oxides, Goodenough's group at the University of Oxford and at the University of Texas at Austin identified three classes of oxide cathodes (layered, spinel, and polyanion) in the 1980s.[10]

The layered oxide cathode $LiCoO_2$ led to a significant increase in cell voltage to ~ 4 V as compared to ~ 2.5 V for the sulfide cathode TiS_2.[32] In pursuit of reducing the cost, Goodenough's group reported $LiMn_2O_4$ cathode with the three-dimensional spinel structure and ~ 4 V.[33] To reduce the cost further, Manthiram and Goodenough explored a series of Fe-containing polyanion hosts $Fe_2(XO_4)_3$ (X = Mo, W, and S).[34,35] They found a significant increase in cell voltage on replacing the oxide anion with a polyanion XO_4: $Fe_2(MoO_4)_3$ (3.0 V), $Fe_2(WO_4)_3$ (3.0 V), and $Fe_2(SO_4)_3$ (3.6 V) compared to < 2.5 V for Fe_2O_3. They attributed the increase in cell voltage to the inductive effect of the polyanion XO_4 that decreases the Fe-O bond covalence and thereby lowers the $Fe^{2+/3+}$ redox energy and increases the cell voltage. Utilizing this concept, Goodenough's group reported $LiFePO_4$ cathode with a cell voltage of ~3.5 V in 1997, which

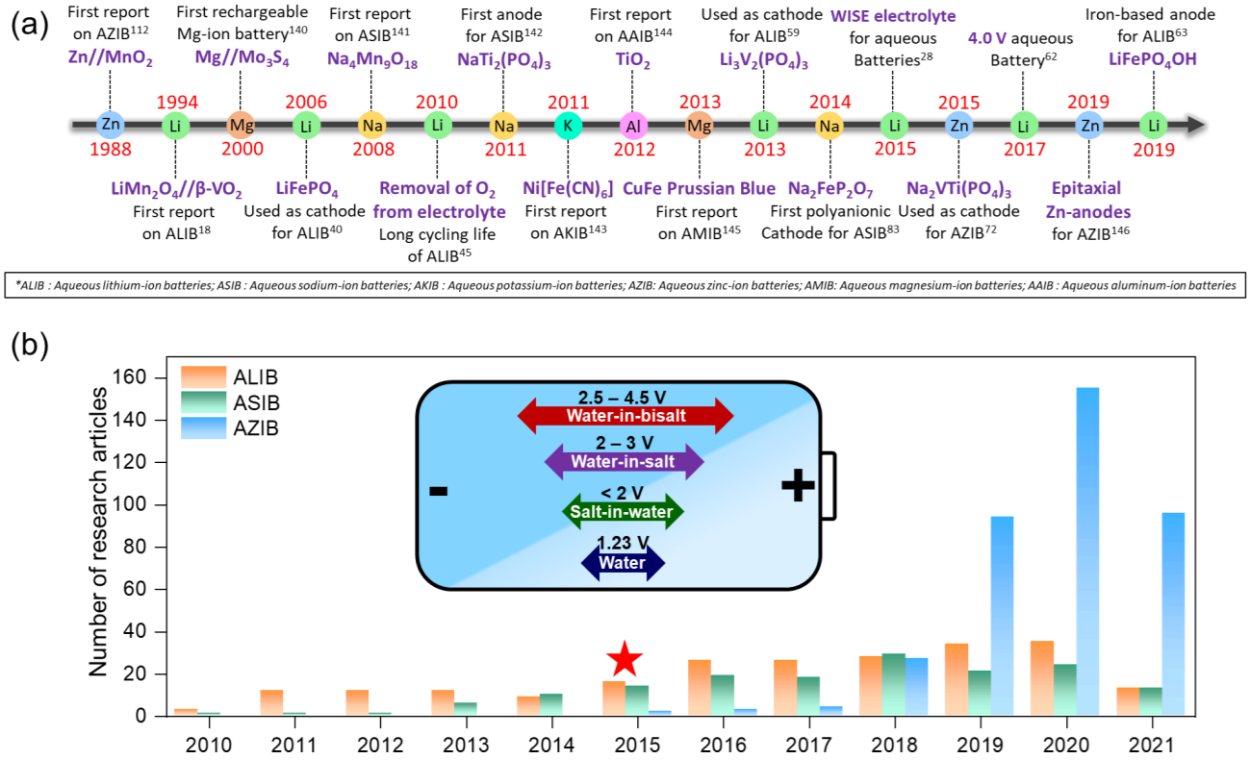

Fig. 1 (a) Timeline depicting some major developments in the field of aqueous batteries. (b) Number of research articles published in the field of aqueous metal-ion batteries (M = Li, Na, and Zn) since 2010. The data were collected from Web of Science on 16 December 2021 by using batteries as the topic filter and aqueous and the corresponding metal-ion as title filter. Inset: Schematic representation of electrochemical operating voltage window of pure water (1.23 V) and different aqueous electrolytes reported in the literature.

was later commercialized.[36] This further fuelled the research on polyanionic materials, and many different classes of polyanionic materials have been explored in the past two decades.[9,37,38] Materials, such as $LiVPO_4F$, $LiV_2(PO_4)_3$, $Na_3V_2(PO_4)_3$, $Na_3V_2(PO_4)_3F_3$, *etc.,* were found to exhibit excellent electrochemical properties for lithium and sodium insertion.[39]

3. Polyanionic cathode materials for aqueous lithium-ion batteries (ALIB)

The concept of lithium intercalation in aqueous media was first reported by Dhan *et al.* in 1994, which opened the floodgate to numerous reports on oxides and polyanionic-based materials both as cathodes and anodes (Fig. 2a).[18] Among the polyanionic materials, many olivine- and NASICON-based materials have been reported in the literature. This section summarizes the developments made in this field in detail.

3.1 Olivine-structured phosphates

Olivine-based $LiFePO_4$ (LFP) is touted as the best polyanionic cathode for commercial applications with organic electrolyte.[36] The material crystallizes in an orthorhombic structure (space group: *Pnma*), with the LiO_6 octahedra forming linear chains along the *b*-axis. The redox potential of LFP lies well within the range of stable operating potential window for ALIBs. The first electrochemical report of LFP in aqueous media came in 2006 by Minakshi *et al.* using saturated aqueous lithium hydroxide (LiOH) as an electrolyte.[40] With cyclic voltammetry, they showed one peak during oxidation while two peaks were recorded during reduction (Fig. 2b). During oxidation, like that in a non-aqueous electrolyte, formation of $FePO_4$ was observed, confirmed by X-ray diffraction (XRD) patterns recorded after oxidation. However, the XRD patterns obtained after reduction showed the presence of Fe_3O_4 species, indicating that the lithium (de)intercalation process is not fully reversible. This was further confirmed by secondary ion mass spectrometry (SIMS), where the Li/Fe ratio was seen to be decreasing during oxidation and increasing during reduction. They observed a specific capacity of 70 mA h g^{-1} with a cathode utilization of 70% in the first cycle. This dropped to 50 mA h g^{-1} (30%) in the second cycle and 40 mA h g^{-1} (20%) in the fifth cycle.

Mi *et al.* tested the electrochemical performance of LFP and Nb-doped LFP in Li_2SO_4 electrolyte with cyclic voltammetry.[41] In the case of LFP, the redox peaks corresponding to the Fe^{2+}/Fe^{3+} redox couple appeared at low and medium scan rates while in the case of Nb-doped LFP, the electrochemical behavior was found to be dependent on the scan rate, indicating a phase transformation in the

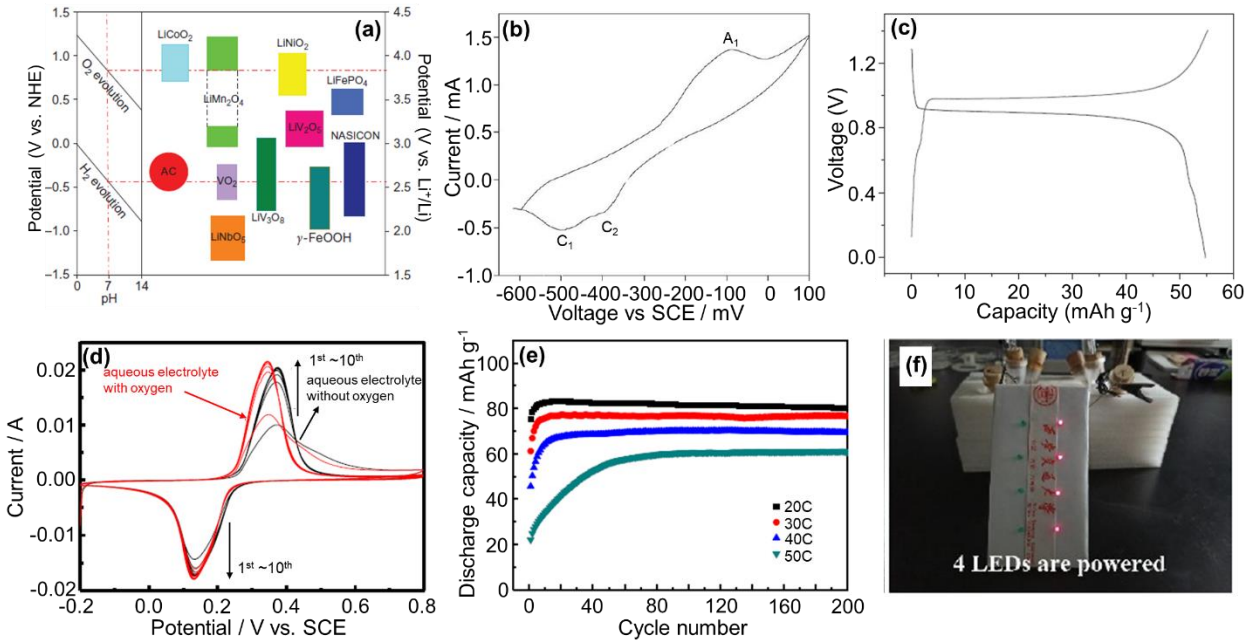

Fig. 2 (a) The redox energies of various materials used as cathode and anode for aqueous lithium-ion batteries. The O_2/H_2 evolution potentials are versus NHE for different pH in 1 M Li_2SO_4 solution while the lithium intercalation potentials of various materials are versus NHE and Li/Li^+. (b) Cyclic voltammogram of $LiFePO_4$ recorded in aqueous lithium hydroxide solution. (c) (Dis)charge profile of LTP||LFP recorded in 1 M Li_2SO_4 aqueous electrolyte (pH = 13) in the absence of oxygen. (d) Cyclic voltammogram of LFP/C recorded at a scan rate of 5 mV s^{-1} with and without oxygen. (e) Rate capability of LFP/C || LiV_3O_8 in 9 M $LiNO_3$ solution without dissolved oxygen at various high C-rates. (f) Practical demonstration of the working of ALIB fabricated with LFP/C/CNTs cathode and zinc-metal anode by powering four LEDs for more than one minute. (a, c) Reproduced with permission from ref 45. Copyright 2010 Nature. (b) Reproduced with permission from ref 40. Copyright 2006 Elsevier. (d, e) Reproduced with permission from ref 47. Copyright 2013 Elsevier. (f) Reproduced with permission from ref 49. Copyright 2020 The Royal Society of Chemistry.

material. He *et al.* tried to understand the intercalation behavior of lithium ion in LFP in both aqueous and non-aqueous media.[42] They observed that the rate capability was much better in aqueous media owing to fast lithium-ion charge transfer at the interface, resulting in a high diffusion coefficient of 2.05 x 10^{-10} cm^2 s^{-1} in a 1 M Li_2SO_4 electrolyte, compared to 4.06 x 10^{-11} cm^2 s^{-1} in a 1 M $LiPF_6$ in propylene carbonate (PC) non-aqueous electrolyte. Using a 0.5 M Li_2SO_4 electrolyte, they obtained a discharge capacity of 141 mA h g^{-1} at 1C rate. The polarization was lower in aqueous electrolyte, implying a low charge-transfer resistance, which was confirmed by electrochemical impedance spectroscopy. A low charge-transfer resistance at the interface and low cell resistance was observed by Tarascon's group while working on carbon-free LFP thin films.[43] Okada's group studied the electrochemical performance of Ni and Mn-doped LFP, i.e., $LiMn_{0.05}Ni_{0.05}Fe_{0.9}PO_4$ cathode coupled with $LiTi_2(PO_4)_3$ (LTP) anode in saturated Li_2SO_4 electrolyte.[44] In the potential window of 0.6 - 1.2 V, the cell delivered a discharge capacity of 104 mA h g^{-1} at 0.2 mA cm^{-2} with good rate capability.

Even though aqueous batteries are safer and non-toxic, they suffer from poor cyclability issues. In 2010, Xia's group came up with a solution to improve the performance by removing oxygen from the electrolyte, using carbon-coated materials and properly adjusting the pH of the electrolyte.[45] They reported that most of the anodes in the discharged state react with oxygen present in the electrolyte. Utilizing LTP as a model, it was demonstrated that the coulombic efficiency is much better in an oxygen-free atmosphere. They also fabricated an LFP | Li_2SO_4 | LTP cell, and it exhibited improved cyclability in a sealed oxygen-free atmosphere. The cell delivered a discharge capacity of 55 mA h g^{-1} and an energy density of 50 W h kg^{-1} at 1C rate when cycled in the potential range of 0 - 1.4 V in 1 M Li_2SO_4 with a pH of 13 (Fig. 2c). The cell also showed excellent cyclability with only 10% capacity loss after 6,000 cycles at 6C rate.

LFP suffers from poor electronic and ionic conductivity, resulting in poor electrochemical performance. Many groups have tried to improve the conductivity by carbon coating, doping, and morphology control. Liu *et al.* reported CeO_2 modified LFP with better ionic conductivity and a high lithium-diffusion coefficient as observed with cyclic voltammetry.[46] Zhao *et al.* reported an aqueous lithium-ion battery assembled with an LFP/C composite as the cathode and LiV_3O_8 as an anode in 9 M $LiNO_3$ electrolyte.[47] The cell delivered an initial discharge capacity of 110 mA h g^{-1} at 1C rate with no dissolved oxygen in the electrolyte. 99% of this capacity was retained after 100 cycles. They also studied the effect of dissolved oxygen in the electrolyte on electrochemical performance (Fig. 2d). In the presence of oxygen, the cell delivered an initial discharge capacity of only 100 mA h g^{-1}, which came down to 70 mA h g^{-1} after

100 cycles at 1C rate. Even at 50C rate, the cell showed a capacity of 61 mA h g^{-1} after 200 cycles (Fig. 2e).

Hou *et al.* reported the stable nature of gel polymer and LISICON-coated lithium-metal anode in aqueous media.[48] They used this anode to fabricate an aqueous battery with macroporous LFP as the cathode and 0.5 M Li_2SO_4 as the electrolyte. The 3-dimensional macroporous nature of the LFP with a pore size of 200 nm assisted the penetration of electrolyte and enhanced the surface area of the electrode-electrolyte interface. The cell delivered a capacity of 105 mA h g^{-1} at a current density of 500 mA g^{-1} with an output voltage of 3.32 V vs. Li^+/Li. Recently, Song *et al.* reported LFP covered with flocculent carbon layers wrapped within CNT as a cathode for ALIB.[49] Using 1 M $ZnSO_4$ + saturated $LiNO_3$ as an electrolyte, the material delivered a discharge capacity of 158 mA h g^{-1} at 1C rate with 100 % retention after 75 cycles. At 50C rate, a discharge capacity of 80 mA h g^{-1} was obtained with 138 % capacity retention after 250 cycles. The presence of carbon layers and CNTs helped in buffering the volume expansion of LFP during lithium (de)intercalation. CNTs also imparted some amorphous nature to the surface and reduced the contact resistance at the electrode-electrolyte interface. The practical application of the battery was demonstrated by lighting four LEDs for more than one minute (Fig. 2f). Among other Fe-based cathodes, Minakshi reported trigonal $FePO_4$ with an amorphous nature showing lithium intercalation properties in LiOH electrolyte with a discharge capacity of 65 mA h g^{-1}.[50]

Apart from LFP, other olivine-structured materials have also been reported for ALIB applications. Minakshi *et al.* reported $LiMnPO_4$ (LMP) for the first time in 2006 using saturated LiOH + 1 M $ZnSO_4$ as an electrolyte.[51] Using CV in saturated LiOH electrolyte, they observed one peak during both anodic and cathodic scans but with a large potential gap, indicating that the lithium (de)intercalation process was slow in this electrolyte. In the potential window of 0.0 - 1.9 V, the Zn | LiOH + $ZnSO_4$ | $LiMnPO_4$ cell showed a cathode material utilization of 44 %, which dropped to 15 % after 20 cycles. XRD showed the formation of $MnPO_4$ upon oxidation and $LiMnPO_4$ upon reduction, indicating reversible lithium intercalation and structural behavior. The behavior is different from LFP, where a mixture of Fe_2O_3 and $LiFePO_4$ were formed after lithium insertion. The same group reported the electrochemical performance of TiS_2 modified LMP as well.[52] They observed that TiS_2 not only reduces polarization but also enhances the discharge capacity. The discharge capacity for 0% and 3% TiS_2-added LMP was found to be, respectively, 70 and 90 mA h g^{-1} when cycled at a current density of 0.5 mA cm^{-2} in LiOH + $ZnSO_4$ electrolyte. Generally, additives in olivine-based LMP materials help in mitigating the Jahn-Teller lattice distortion, but in this system, this was not the case. Rather, TiS_2 assisted in suppressing proton insertion in the material. Using CV, Manjunatha *et al.* showed that proton insertion is the dominant process at lower lithium concentrations in the electrolyte.[53] However, using saturated or highly concentrated electrolytes, lithium-ion insertion becomes dominant along with some amount of proton insertion. They assembled an LTP | 5 M $LiNO_3$ | LMP cell, which delivered a discharge capacity of 84 mA h g^{-1} at C/5 rate with good cyclability until 50 cycles.

Zhao *et al.* reported $LiFe_{0.5}Mn_{0.5}PO_4$ with a slightly distorted crystal structure compared to pristine LMP in saturated $LiNO_3$ electrolyte.[54] The $LiFe_{0.5}Mn_{0.5}PO_4$//LiV_3O_8 cell delivered an initial discharge capacity of 107 mA h g^{-1} at C/10 rate (Fig. 3a). The discharge curves exhibited two plateaus corresponding to Fe^{2+}/Fe^{3+} and Mn^{2+}/Mn^{3+} redox. However, using energy-dispersive X-ray spectroscopy (EDS), manganese dissolution was observed. Interestingly, the cell exhibited poor cyclability at lower C-rates, while the capacity retention was much better at higher C-rates (Fig. 3b). Even at 50C rate, the cell delivered a discharge capacity of 67 mA h g^{-1}. Zhao *et al.* reported olivine-based $LiMn_{1-x}Fe_xPO_4$/C (x = 0.5, 0.4, 0.3, 0.2) with a similar morphology as a cathode in an $LiNO_3$ aqueous electrolyte.[55] They observed that the electrochemical performance of the material was much better in electrolytes with no dissolved oxygen, as reported by other groups for LFP cathodes. This was attributed to low charge-transfer resistance and enhanced lithium diffusion coefficients. Among the four materials, at C/10 rate, $LiMn_{0.6}Fe_{0.4}PO_4$ delivered the maximum discharge capacity of 111 mA h g^{-1} in an electrolyte with oxygen which increased to 112 mA h g^{-1} in an electrolyte with no dissolved oxygen. The effect of oxygen on electrochemical performance was much more pronounced in other materials.

Minakshi *et al.* reported $LiCoPO_4$ with an aqueous LiOH electrolyte and tin-metal (Sn) anode.[56] The material delivered a discharge capacity of 82 mA h g^{-1} at a current density of 0.5 mA cm^{-2}, with a high polarization potential of 0.5 V (Fig. 3c). The *ex-situ* XRD at the fully charged state indicated both $LiCoPO_4$ and $CoPO_4$ species, unlike that with LFP and LMP, where $FePO_4$ and $MnPO_4$ were obtained. This implies partial delithiation during charging; however, the peaks corresponding to $CoPO_4$ completely disappeared upon discharge and the pristine phase was recovered. Minakshi *et al.* also reported $LiNiPO_4$ as a cathode using similar electrochemical conditions to those of $LiCoPO_4$.[57] This material showed electrochemical activity with very high polarization and only 45% coulombic efficiency, but with decent capacity retention (Fig. 3d). Upon charging, formation of amorphous delithiated $NiPO_4$ and a small amount of β-NiOOH was observed. Reversible lithium transfer between $LiCo_{0.5}Ni_{0.5}PO_4$ (isostructural to $LiCoPO_4$ and $LiNiPO_4$) and LiOH was also demonstrated by Minakshi *et al.*[58]

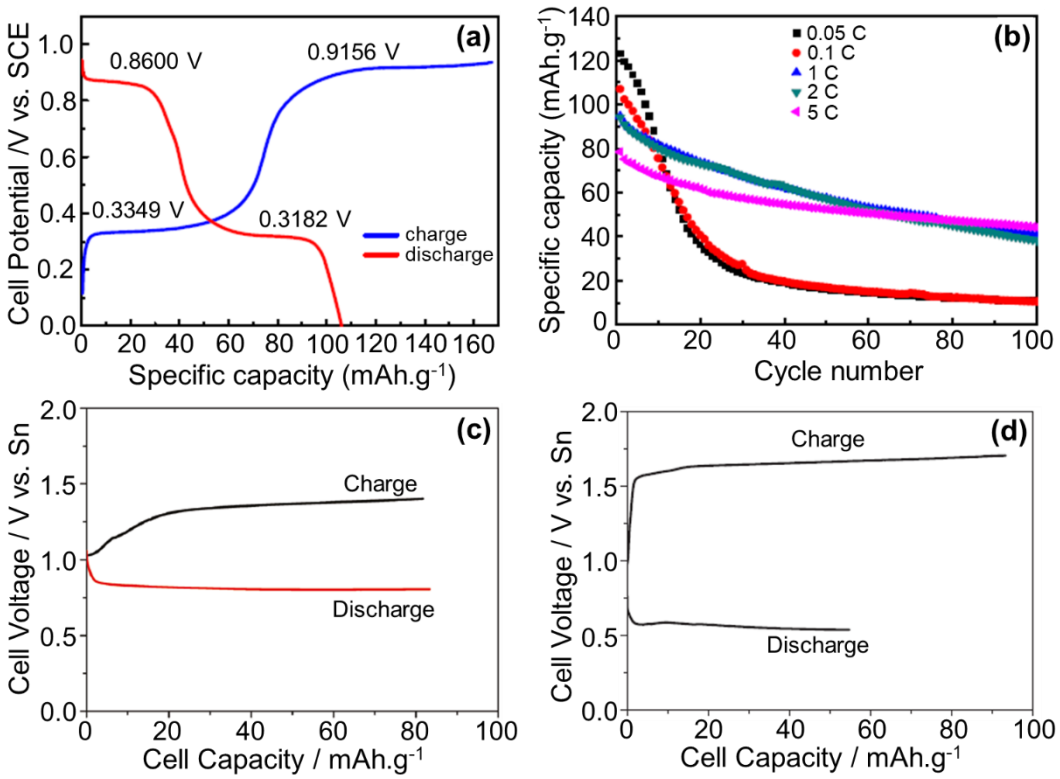

Fig. 3 (a) (Dis)charge profile of a $LiFe_{0.5}Mn_{0.5}PO_4/C||LiV_3O_8$ cell at C/10 rate. (b) Cyclability of a $LiFe_{0.5}Mn_{0.5}PO_4/C||LiV_3O_8$ cell at different C-rates for 100 cycles. (c) First (dis)charge profile of a $LiCoPO_4$ cell with LiOH aqueous electrolyte at a current density of 0.5 mA cm^{-2}. (d) First (dis)charge profile of a $LiNiPO_4$ cell with LiOH aqueous electrolyte at a current density of 0.5 mA cm^{-2}. (a, b) Reproduced with permission from ref 54. Copyright 2012 Elsevier. (c) Reproduced with permission from ref 56. Copyright 2011 American Chemical Society. (d) Reproduced with permission from ref 57. Copyright 2011 Elsevier.

3.2 Vanadium-based materials

Apart from olivine-based materials, monoclinic $Li_3V_2(PO_4)_3$ (LVP) has also been reported as a cathode for ALIB. The material crystallizes in a monoclinic structure (space group: $P2_1/n$), in which each VO_6 octahedron is surrounded by six PO_4 tetrahedra and each PO_4 tetrahedron is surrounded by four VO_6 octahedra. The first report came in 2013 when Jiang *et al.* reported lithium (de)insertion in the material in 2 M Li_2SO_4 as an electrolyte in the potential range of -0.2 to 0.8 V vs. SCE.[59] They fabricated an activated carbon (AC)//LVP asymmetric hybrid capacitor. When cycled in the potential range of 0.0 – 1.7 V, sloping (dis)charge profiles were observed and 90 % of the capacity was retained after 1,000 cycles at a current density of 250 mA g^{-1}. An energy density of 35 W h kg^{-1} was obtained at a power density of 102 W kg^{-1}. The report was mainly focused on capacitor fabrication. The initial electrochemical report of LVP was reported by Lin *et al.* in a saturated $LiNO_3$ electrolyte.[60] In the potential window of 0.25 – 1.35 V vs. SHE, the material delivered a discharge capacity of 100 mA h g^{-1} at 5C rate. The discharge profiles exhibited three voltage plateaus corresponding to a single-phase transition among $Li_{3-x}V_2(PO_4)_3$ with x = 0, 0.5, 1, and 2 (Fig. 4a). The effect of pH on the electrolyte was also studied. In neutral and basic electrolytes, capacity fading was observed, while capacity retention was better in a slightly acidic electrolyte (pH = 5) (Fig. 4b).

The capacity fading was further investigated by Wang *et al.,* and LVP dissolution and structural deterioration were found to be the main reasons for the fading.[61] This was improved by employing WISE, and they fabricated a LVP//LTP cell with 21 m LiTFSI electrolyte. The cyclability of the cell assembled in the mass ratio of 2 : 1 (LVP : LTP) delivered a much better capacity compared to that of a cell assembled with the ratio of 1 : 1 (Fig. 4c). The cell delivered a specific capacity of 123 mA h g^{-1} at C/10 rate and 113 mA h g^{-1} at 1C rate. Even at -20°C, the cell delivered a capacity of 111 mA h g^{-1} at C/5 rate and 60% capacity was retained at 6C rate.

The electrochemical stability window of water is ~ 1.23 V, which corresponds to a cathodic and anodic limit of, respectively, 2.62 V and 3.85 V vs. Li at a pH of 7, implying that various chemistries like graphite (0.10 V), $LiMnO_2$ (4.10 V), and $LiNi_{1/3}Mn_{1/3}Co_{1/3}O_2$ (4.20

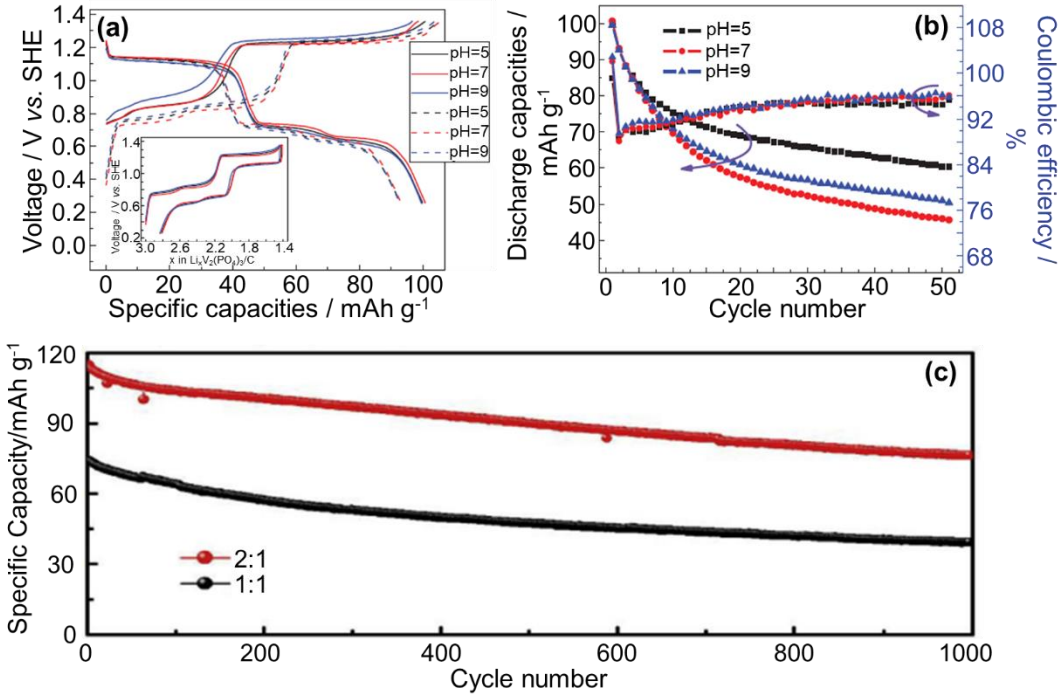

Fig. 4 (a) Electrochemical performance of LVP/C recorded in saturated $LiNO_3$ electrolyte at different pH values and 5C rate. (b) Cyclability and coulombic efficiency of LVP/C recorded in saturated $LiNO_3$ electrolyte at different pH values. (c) Comparison of the cyclability of LVP||LTP full cells assembled in a mass ratio of 1 : 1 and 2 : 1 while cycled at 1C rate with 21 M LiTFSI electrolyte. (a, b) Reproduced with permission from ref 60. Copyright 2014 The Electrochemical Society. (c) Reproduced with permission from ref 61. Copyright 2018 Elsevier.

V), *etc.* are out of scope of these limits. However, with WISE both anodic and cathodic limits are extended. In such high concentrated electrolytes, the water molecules have asymmetrical rearrangement at the inner-Helmholtz layer of the electrode when potential is applied. Using molecular dynamics calculations, it was observed that at 2.5 V, the salts dominate the inner-Helmholtz layer with negligible contact of water with the graphite surface.[62] This favours the formation of SEI. However, on further reducing the anodic limit to 0.5 V, the salts experience repulsion and more water molecules are exposed to the surface, leading to onset of hydrogen evolution, which makes it difficult to use anodes like graphite, silicon or lithium metal. However, Wang and co-workers found a strategy to utilize graphite or lithium-metal anode by using an immiscible hydrophobic additive as a thin gel coating on the surface of anode. This additive decomposes into LiF and C-F species upon lithiation of anode, assisting in reversible cycling in aqueous electrolytes. They used a highly fluorinated 1,1,2,2-Tetrafluoroethyl-2,2,2-trifluoroethyl ether (HFE) as an additive and formed a gel by mixing it with 0.5 M LiTFSI. The CV of the gel-coated graphite showed a peak in the first cathodic scan, which was associated with interphase formation. This peak was not observed in subsequent cycles indicating the irreversible process of interphase formation. A 4.0 V, the ALIB was reported by coupling the anode with $LiVPO_4F$ cathode with a first discharge capacity of > 275 mA h g^{-1} at 0.3C rate. The cyclability of the cell was checked up to 50 cycles and a discharge capacity of > 240 mA h g^{-1} was obtained at the end of 50th cycle. Even though vanadium-based materials are generally associated with toxicity and low structural stability in aqueous electrolytes, the reports mentioned above showcase the potential use of these materials, especially LVP, for grid storage applications.

3.3 Other polyanionic materials

Recently, *tavorite*-structured $LiFePO_4OH$ has been reported as an anode for ALIB.[63] The hydrothermally synthesized material delivered a discharge capacity of 140 mA h g^{-1} when cycled in the potential window from 2.2 to 4.2 V vs Li^+/Li at a current density of 1.0 mA cm^{-2} in 1 M $LiPF_6$ in ethylene carbonate (EC)/dimethyl carbonate (DMC) organic electrolyte. 99% of the initial discharge capacity was retained after 60 cycles. For the aqueous battery measurements, a three-electrode set up was used with Zn-metal as the counter electrode, Ag-AgCl/saturated KCl as the reference electrode and LFPOH as the working electrode. In a concentrated 21 m LiTFSI + 7 m LiOTf electrolyte, a discharge capacity of 153 mA h g^{-1} was obtained at a potential of -0.3 to -0.4 vs. Ag/AgCl. 81% of the capacity was retained after 50 cycles with the discharge profiles similar to that in organic electrolytes. The operating voltage was lying in the anodic range of ALIB, and a full-cell was assembled with LFP, which delivered a discharge capacity of 121 mA h g^{-1} at 0.8 V with an energy density of 97 W h kg^{-1}. The electrochemical performances of the polyanionic cathode materials for ALIB applications are summarized in Table 2.

Table 2. Overview of the electrochemical performances of polyanionic cathode materials for aqueous lithium-ion batteries.

Material/System	Electrolyte	Capacity/ mA h g^{-1} (C-rate)	% Capacity retention (cycle number)	Voltage (Energy density)	Ref
$LiFePO_4$	0.5 M Li_2SO_4	141 (1 C)	-	0.16 V vs. SCE	42
LTP//$LiMn_{0.05}Ni_{0.05}Fe_{0.9}PO_4$	sat. Li_2SO_4	87 (0.2 mA cm^{-2})	~63 (50) @0.2 mA cm^{-2}	-	44
$LiTi_2(PO_4)_3$//$LiFePO_4$	1 M Li_2SO_4	55 (1 C)	90 (1000) @6 C	0.9 V (50 W h kg^{-1})	45
LiV_3O_8//$LiFePO_4$/C	9 M $LiNO_3$	110 (1 C)	99 (100) @10 C	-	47
Macroporous $LiFePO_4$	0.5 M Li_2SO_4	106 (100 mA g^{-1})	~99 (50) @100 mA g^{-1}	3.32 V vs. Li^+/Li (342 W h kg^{-1})	48
Zn//$LiFePO_4$/C/CNTs	1 M $ZnSO_4$ + sat. $LiNO_3$	158 (1 C)	100 (75) @1 C	1.23 V (194 W h kg^{-1})	49
Zn//$FePO_4$	5 M LiOH	65 (0.5 mA cm^{-2})	-	-	50
Zn//TiS_2 modified $LiMnPO_4$	aq. LiOH	90 (0.5 mA cm^{-2})	80 (20) @0.5 mA cm^{-2}	-	52
LiV_3O_8//$LiFe_{0.5}Mn_{0.5}PO_4$/C	sat. $LiNO_3$	123.09 (0.05 C)	56 (100) @5 C	-	54
Sn//$LiCoPO_4$	aq. LiOH	82 (0.5 mA cm^{-2})	85 (25) @0.5 mA cm^{-2}	-	56
$Li_3V_2(PO_4)_3$/C	2 M Li_2SO_4	68.2 (100 mA g^{-1})	-	-	59
$Li_3V_2(PO_4)_3$/C	sat. $LiNO_3$	100 (5 C)	60 (50) @5 C	-	60
LTP//$Li_3V_2(PO_4)_3$	21 m LiTFSI	123 (0.1 C @ RT) 111 (0.2 C @ -20 °C)	65 (1000) @1 C	1.25 V	61
$LiFePO_4OH$	21 m LiTFSI + 7 m LiOTf	153 (1.0 mA cm^{-2})	81 (50) @1.0 mA cm^{-2}	-0.3 to -0.4 V vs. Ag/AgCl	63

* LTP = $LiTi_2(PO_4)_3$; Zn = Zinc; Sn = Tin; LiTFSI = $LiN(CF_3SO_2)_2$; LiOTf = $Li(CF_3SO_3)$; aq. = aqueous; sat. = saturated; Ref = Reference

4. Polyanionic cathode materials for aqueous sodium-ion batteries (ASIB)

Sodium-ion batteries have emerged as the best alternative in the post-lithium-ion batteries era owing to the low cost, high abundance, and promising application for grid storage. Along with organic electrolyte-based batteries, aqueous sodium-ion batteries (ASIB) have received significant attention in the past decade. Multiple classes of cathode materials have been explored, such as manganese-based oxides, Prussian blue analogs, *etc.*[20,22] Of late, many polyanionic materials have also been explored owing to their tunable redox potential and high structural stability. This section provides a detailed review of the different polyanionic classes of materials reported as cathodes for ASIB.

4.1 Vanadium-based phosphates

NASICON based $Na_3V_2(PO_4)_3$ (NVP) has been reported to exhibit the best performance for sodium (de)intercalation in organic electrolytes.[64,65] The material crystallizes in an open 3D structure showing corner-shared PO_4 tetrahedra and VO_6 octahedra. The large tunnels are able to accommodate large Na-ions and enables perturbation-free diffusion in the structure. The material was first studied for ASIB applications in 2014 by Song *et al.* by employing 1 M Na_2SO_4 electrolyte in a three-electrode system.[66] They initially recorded the CV of the material in neutral 1 M Li_2SO_4, 1 M Na_2SO_4, and 1 M K_2SO_4 electrolyte. Redox peaks were observed in all three electrolytes, but the peaks were asymmetric in lithium and potassium-based electrolytes, indicating irreversible ion (de)intercalation. The peak separations were 704, 512, and 600 mV, respectively, in lithium, sodium, and potassium-based electrolytes

confirming that Na-intercalation in NVP is more facile. A linear relationship between the square root of scan rate and peak current indicated a diffusion-controlled electrochemical behavior. The capacitive properties of NVP were studied by cycling between 0 to 0.9 V vs. SCE, where a capacitance of 209 F g^{-1} was obtained at a current density of 1 A g^{-1}. Poor cycling stability was observed due to cathode dissolution and water oxidation. Zhang *et al.* studied the sol-gel synthesized carbon-coated NVP nanocomposite as a cathode in 1 M Na_2SO_4 as an electrolyte.[67] On cycling at 0 - 0.9 V vs. SCE, the material delivered an initial discharge capacity of 95 mA h g^{-1} at 10C rate. The high capacity was attributed to nano-sized grains and carbon coating. However, they also observed capacity fading due to cathode dissolution, which was evident by a change in the color of the electrolyte from colorless to yellow.

Li *et al.* fabricated $NaTi_2(PO_4)_3$ (NTP)||NVP full-cells in a mass ratio of 8 : 7 (anode excess) with 1 M Na_2SO_4 electrolyte and obtained a discharge capacity of 71 mA h g^{-1} at a current density of 2 A g^{-1} when cycled between 0.5 to 1.6 V, albeit poor cycling stability due to cathode dissolution.[68] The cell managed to deliver a capacity of 58 mA h g^{-1} at a current density of 10 A g^{-1} with much better rate performance. A high energy density of 29 W h kg^{-1} at a power density of 5145 W kg^{-1} was obtained. During the same year, Li *et al.* fabricated a cell with carbon and reduced graphene oxide (rGO) incorporated cathode and zinc-metal as an anode with 0.5 M $CH_3COONa/Zn(CH_3COO)_2$ electrolyte.[69] On cycling at 0.8 – 1.7 V vs. Zn^{2+}/Zn, a discharge capacity of 91 mA h g^{-1} at C/2 rate was obtained with a stable output voltage of 1.42 V. Even at 20C rate, a discharge capacity of 60 mA h g^{-1} was obtained. Although it was a hybrid battery system, only Na^+ (de)insertion was observed, which was further evident by similar (dis)charge plateaus in aqueous and organic (1 M $NaClO_4$ in PC) electrolytes. The effect of only carbon and carbon + rGO was also studied. The discharge capacity and capacity retention of carbon + rGO incorporated material were higher than that of only carbon incorporated NVP. Electrochemical impedance spectroscopy analysis showed a lower charge-transfer resistance for carbon + rGO incorporated NVP along with a lower Warburg coefficient, indicating better Na^+ ion kinetics. Recently, a low-cost 17 m $NaClO_4$ + 2 m NaOTF WISE electrolyte was reported, where $NaClO_4$ helped in reducing the water activity and NaOTF assisted in SEI formation. With X-ray photoelectron spectroscopy (XPS) and time-of-flight secondary ion mass spectrometry (TOF-SIMS), a NaF-Na_2O-NaOH SEI was observed on the anode. The electrolyte resulted in a 1.75 V symmetric NVP@C||NVP@C cell with a high energy density of 70 W h kg^{-1} and 87.5% capacity retention after 100 cycles at 1 C rate.[70] A multi-component aqueous electrolyte (MCAE) of $NaClO_4$-H_2O-Urea-DMF was reported for its low cost, non-toxic, and wide-temperature characteristics.[71] The electrolyte forms a composite solvent sheath leading to generation of uniform SEI layer, hence enhancing the electrochemical stability window to 2.8 V. A 1.2 V NVP/NTP battery was assembled with the electrolyte with 80 % capacity retention after 2,000 cycles at 2C rate.

All reports mentioned above indicate that the structural instability of NVP in aqueous electrolytes leads to poor cyclability. A way to circumvent this issue is cationic substitutions. Mason *et al.* reported Ti substituted NVP, giving rise to $Na_2VTi(PO_4)_3$ (NVTP), where half of the vanadium sites are substituted by titanium.[72] Ti^{4+} is insoluble in water as it forms oxides with various levels of hydration. Hence, in aqueous electrolytes, it passivates itself from the attack by electrolytes. Cyclic voltammetry confirmed the high structural stability of NVTP, where even after 100 cycles, the redox peaks were stable, whereas the redox peaks of NVP disappeared after five cycles (Fig. 5a,b). When cycled at 0.1 - 0.45 V vs. Ag/AgCl, the material delivered a discharge capacity of 55 mA h g^{-1} at 2C rate, 98% of which was retained after 100 cycles in 1 M Na_2SO_4 electrolyte. Pouch cells were also assembled with two different anodes namely activated carbon (AC) and NTP. The cell with AC as an anode exhibited hybrid battery/supercapacitor type behavior. During the first discharge, 8 % of the first charge capacity was lost, and 84 % was retained after 100 cycles at 1C rate. In contrast, the cell with NTP as an anode exhibited fast capacity fade, which was attributed to the presence of oxygen in the electrolyte and hydrogen evolution. Utilizing the V^{4+}/V^{3+} and Ti^{4+}/Ti^{3+} redox couples, there are some reports of symmetric cells that were fabricated with NVTP as a cathode as well as an anode. The first report came in 2017 when cross-linked NVTP@C nanofibers were used as bifunctional electrodes for symmetric ASIB.[73] Wang *et al.* used NVTP as a cathode utilizing the V^{4+}/V^{3+} redox couple, and a discharge capacity of 56 mA h g^{-1} was obtained at 1C rate on cycling at 0.0 - 0.6 V vs. Ag/AgCl (Fig. 5c).[74] The XRD pattern was recorded up to 0.6 V and the peaks shifted to higher 2θ values indicating volume shrinkage due to the extraction of sodium ions. The material exhibited good cathode performance with a slight capacity decay after 500 cycles at 5C rate. The anodic performance of the material was checked by cycling the material from -0.8 to 0.0 V vs. Ag/AgCl, and it exhibited a discharge capacity of 51 mA h g^{-1} at 1C rate (Fig. 5d). Negligible capacity loss was observed at 5C rate after 500 cycles. A symmetric cell was fabricated, and it delivered a discharge capacity of 50 mA h g^{-1} and an energy density of 30 W h kg^{-1} at 1C rate when cycled in the potential window of 0.2 to 1.5 V using 1 M Na_2SO_4 as an electrolyte (Fig. 5e). Even at 10C rate, 70% of the capacity was retained after 1,000 cycles. Passerini's group also fabricated a symmetric cell with NVTP material and studied the effect of the concentration of $NaClO_4$ electrolyte and a "*water-in-salt*" NaOTf electrolyte on the electrochemical performance.[75] The electrochemical performance was better in highly concentrated 8 M $NaClO_4$ electrolyte and 9.2 m NaOTf "*water-in-salt*" electrolyte. The better performance was attributed to the formation of a resistive, but protective interface layer. Excellent cycling stability was seen in 9.2 m NaOTf electrolyte with a minimal capacity loss after 1,000 cycles at 20C rate. Recently, Nakamoto and co-workers reported 26 m sodium trifluoroacetate (NaTFA) concentrated electrolyte with an electrochemical stability window of 3.1 V and used it to fabricate a symmetric cell with NVTP.[76] The performance was compared with 17 m $NaClO_4$ electrolyte. Although the half-cells showed identical behavior in both electrolytes, the voltage profiles were different for full cells after 50 cycles. While the profiles were unchanged after 50

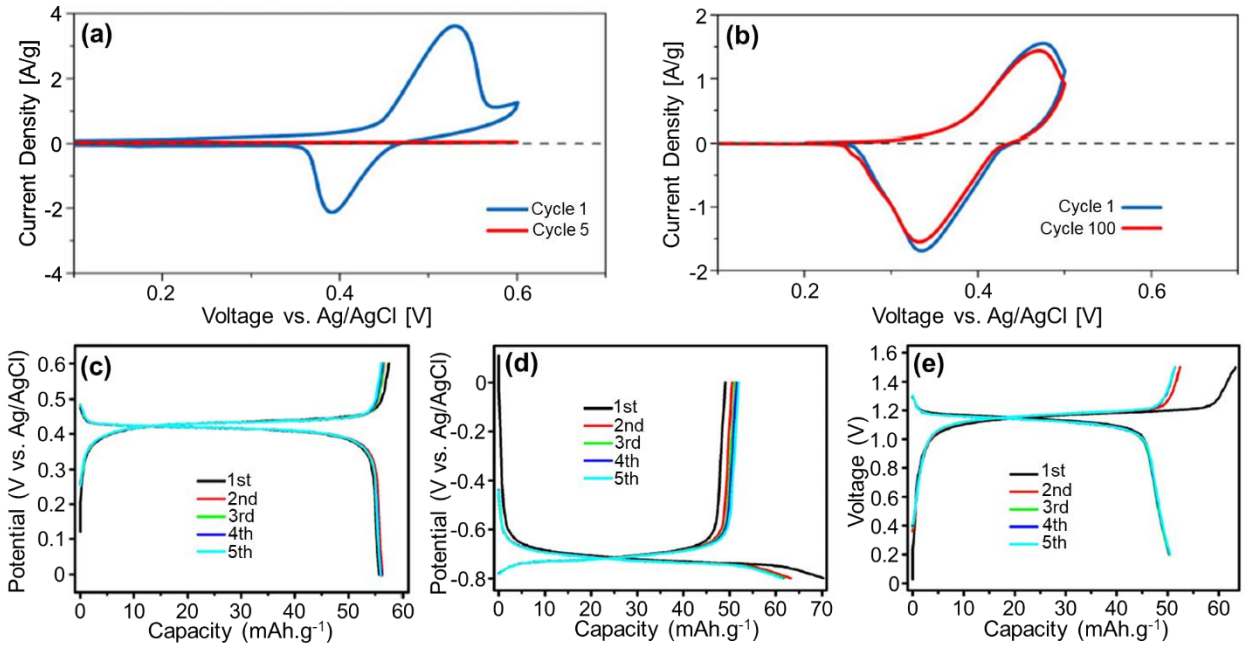

Fig. 5 (a) Cyclic voltammogram (CV) of $Na_3V_2(PO_4)_3$ in 1 M Na_2SO_4 electrolyte at a scan rate of 0.5 mV s^{-1}, depicting the disappearance of redox peaks after five cycles attributed to the structural instability of the material. (b) CV of $Na_2VTi(PO_4)_3$ (NVTP) in 1 M Na_2SO_4 electrolyte at a scan rate of 0.5 mV s^{-1}, showing the structural stability of the material even after 100 cycles. (c, d) Electrochemical performance of NVTP as a cathode and anode, respectively, utilizing V^{3+}/V^{4+} and Ti^{4+}/Ti^{3+} redox couples at 1C rate. (e) Electrochemical performance of a symmetric cell fabricated with NVTP at 1C scan rate. (a, b) Reproduced with permission from ref 72. Copyright 2015 The Electrochemical Society. (c, d, e) Reproduced with permission from ref 74. Copyright 2018 Springer.

cycles in 26 m NaTFA electrolyte, the higher plateau disappeared after 50th cycle in 17 m $NaClO_4$ electrolyte, leading to capacity fade. This was attributed to less acidic nature, small mole fraction of water, and a robust fluoride layer formation at anode due to which the "*water-in-salt*" effect was more pronounced.

4.2. Fluorophosphate-based materials

Another class of materials that have been explored as cathodes for ASIB are fluorophosphates. Fluorine is the most electronegative element in the periodic table, hence, when coupled with the inductive effect of the PO_4-group, it imparts a more ionic nature to the M-O bonds, leading to increased cell voltage.[39] The first report of fluorophosphate cathode for aqueous batteries came in 2014 when $NaVPO_4F$ was used to fabricate a full cell with a polyimide anode.[77] The CV of the material in 5 M $NaNO_3$ electrolyte displayed two redox peaks corresponding to two different Na (de)intercalation processes. The material delivered a discharge capacity of 54 mA h g^{-1} when cycled at 0.0 - 1.0 V vs. SCE at a current density of 50 mA g^{-1}. The full cell assembled in a mass ratio of polyimide : $NaVPO_4F$ = 3 : 1 delivered an initial discharge capacity of 40 mA h g^{-1}, which came down to 30 mA h g^{-1} after the 20th cycle. The capacity fading of the full cell was due to $NaVPO_4F$, as it was observed that the capacity retention of the cathode was poor while the anode exhibited good capacity retention individually.

Kumar *et al.* investigated the electrochemical performance of $Na_3V_2O_{2x}(PO_4)_2F_{3-2x}$/multi-walled carbon nanotube (MWCNT) cathode in both aqueous and non-aqueous electrolytes.[78] From synchrotron X-ray analysis, it was observed that the material consisted of a mixed phase of both $Na_3V_2(PO_4)_2F_3$ (space group: $P4_2/mnm$) and $Na_3V_2O_2(PO_4)_2F$ (space group: $I4/mmm$). Using ^{23}Na solid-state nuclear magnetic resonance (NMR), they proposed $Na_3V_2O_{0.92}(PO_4)_2F_{2.08}$ as the general formula of the prepared material. The CV of the material in non-aqueous electrolyte exhibited two redox peaks corresponding to two-sodium ion (de)intercalation from the structure (Fig. 6a). In comparison, the CV in 10 M $NaClO_4$ aqueous electrolyte exhibited a single redox peak in the voltage range of 0.0 to 0.9 V vs. SCE, indicating a single sodium utilization in the material (Fig. 6b). The voltage window was kept narrow to avoid water oxidation. The electrochemical performance of the material as studied in a beaker-type cell and a discharge capacity of 46 mA h g^{-1} was observed at 1C rate operating at a high potential of 0.95 V vs. SCE. Even at 40C rate, 40% of the discharge capacity at 1C rate was obtained, and *ex-situ* scanning electron micrographs confirmed high structural stability. Two types of full cells were assembled with Zn and NTP/C as an anode. The former delivered a discharge capacity of 54 mA h g^{-1} at 1C rate, and 85% was retained after 400 cycles. The discharge voltage was 1.65 V with an energy density of 84 W h kg^{-1}. In contrast, the full cell with NTP/C anode exhibited a discharge capacity of 30 mA h g^{-1} after 400 cycles at 10C rate.

Later they also studied the effect of electrolyte additives on the electrochemical performance of the same material.[79] They observed that high ionic mobility and low dissolved oxygen are the reason for good electrochemical performance in 10 M $NaClO_4$ electrolyte. However, a 2 vol.% addition of vinylene carbonate (VC) further improved the performance as it lowered the pH of the electrolyte to 1.7, which assisted the formation of a passivation layer at the interface, avoiding side reactions. The group also reported on the electrochemical performance of $Na_3V_2O_2(PO_4)_2F$-MWCNT, which achieved a discharge capacity of 35 mA h g^{-1} at 1C rate for the half-cell configuration. In a full cell configuration with NTP-MWCNT anode, 42 mA h g^{-1} was obtained at the end of 100 cycles (Fig. 6c).[80] Liu *et al.* reported the electrochemical performance of full cell assembled with $Na_3V_2(PO_4)_2F_3$ single-walled carbon nanotube (SWCNT) cathode and NTP-MWCNT anode in highly concentrated 17 m $NaClO_4$ electrolyte.[81] The cell delivered an energy density of 150 W h kg^{-1} at a high voltage of 1.92 V with an initial discharge capacity of 81 mA h g^{-1}. Recently Sharma *et al.* investigated the electrochemical performance of Na_2FePO_4F cathode in 17 m $NaClO_4$ aqueous electrolyte.[82] A discharge capacity of 84 mA h g^{-1} was obtained in the half cell configuration when cycled in the potential window of -0.9 to 0.9 V vs. Ag/AgCl at a current density of 1 mA cm^{-2} with good cycling stability up to 100 cycles. The full-cell assembled with NTP anode delivered a discharge capacity of 85 mA h g^{-1} at an average cell potential of 0.7 V.

4.3. Other polyanionic materials

Apart from NASICON based vanadium phosphates and fluorophosphates, other polyanionic and mixed polyanionic materials have also been explored for ASIB. Jung *et al.* reported $Na_2FeP_2O_7$ pyrophosphate in 2014 as a cathode for ASIB application.[83] The material crystallizes in a triclinic structure (space group: *P*-1) with a 3-dimensional framework. When cycled between -0.2 to 0.7 V vs. SCE, the material delivered a discharge capacity of 65 mA h g^{-1} at C/5 rate. 86% of the capacity was retained at the end of 300 cycles at 1C rate. Okada's group fabricated $Na_2FeP_2O_7$ || NTP full cell and examined the effect of different electrolytes on the electrochemical performance.[84] They observed that full-cells with 2 M Na_2SO_4 and 4 M $NaClO_4$ electrolyte exhibited much better performance than non-aqueous electrolytes due to their high relative dielectric constant and lower viscosity of water, while in the case of 4 M $NaNO_3$, a large irreversible capacity was observed due to corrosive side reactions and H_2 gas evolution. Goodenough's group reported another NASICON-type $Na_3MnTi(PO_4)_3$ and fabricated a symmetric cell with 1 M Na_2SO_4 electrolyte.[85] It has a three-dimensional structure consisting of MnO_6 and TiO_6 octahedra sharing corners with PO_4 tetrahedra, resulting in two sodium sites. As a cathode, the material delivered a discharge capacity of 58 mA h g^{-1} at C/2 rate when cycled between 0.0 to 1.0 V vs. Ag/AgCl, utilizing the Mn^{2+}/Mn^{3+} redox couple (Fig. 6d). Whereas as an anode, a discharge capacity of 58 mA h g^{-1} was obtained at C/2 rate when cycled at -1.3 to 0.0 V vs. Ag/AgCl by utilizing the Ti^{4+}/Ti^{3+} redox couple (Fig. 6e). The symmetric cell was cycled between 0.4 to 1.8 V vs. Ag/AgCl, and a discharge capacity of 58 mA h g^{-1} was obtained at C/2 rate with an energy density of 40 W h kg^{-1}. A discharge capacity of 57 mA h g^{-1} was obtained at a 1C rate, and 98% was retained after 100 cycles.

Another NASICON type $Na_4MnV(PO_4)_3$-rGO cathode was reported as a cathode for ASIB in 10 M $NaClO_4$ with 2% VC additive as an electrolyte.[86] The half-cell delivered a discharge capacity of 92 mA h g^{-1} at 1C rate when cycled between 0.0 and 0.82 V vs. Ag/AgCl with an average potential of 0.66 V vs. Ag/AgCl. Full-cells assembled with NTP-MWCNT anode delivered a discharge capacity of 97 mA h g^{-1} at 10C rate when cycled between 0.8 and 1.65 V with an average cell potential of 1.30 V and an energy density of 130 W h kg^{-1}. Electrochemical properties of $Na_3MnCO_3PO_4$ carbonophosphate with the *sedorenkite* structure (space group: $P2_1/m$) in 17 m $NaClO_4$ aqueous electrolyte were first explored by Xie and co-workers.[87] A discharge capacity of 134 mA h g^{-1} was observed at a high current density of 2 mA cm^{-2}, owing to the high ionic conductivity of 17 m $NaClO_4$ aqueous electrolyte (108 mS cm^{-1}) as compared to 1 M $NaPF_6$ in EC:DMC (1:1 v/v) organic electrolyte (6.5 mS cm^{-1}). Shiprath *et al.* also tried to study the electrochemical performance of the material in 5 M $NaNO_3$ electrolyte.[88] The full cell assembled with NTP anode delivered an initial discharge capacity of 77 mA h g^{-1} at C/5 rate, and 89% was retained after 100 cycles (Fig. 6f). The coulombic efficiency was found to be low for the initial cycle, which was attributed to the difficulty in the intercalation of Na^+ ions into the lattice along with poor electronic conductivity of the material. Lately, the iron-analogue of the carbonophosphate, *i.e.*, $Na_3FeCO_3PO_4$ have also been explored for ASIB applications.[89,90] Xie and co-workers also studied the performance of $Na_3FeCO_3PO_4$//$NaTi_2(PO_4)_3$ in 17 m $NaClO_4$ aqueous electrolyte and achieved a high discharge capacity of 161 mA h g^{-1} at current density of 2 mA cm^{-2} with 65.6 % retention after 30 cycles.[89] $Na_7V_4(P_2O_7)_4(PO_4)$ nano-rods with carbon coating exhibiting a tetragonal structure and high operating potential have also been explored as a cathode for ASIB.[91] With 1 M Na_2SO_4 electrolyte, the material delivered a discharge capacity of 37 mA h g^{-1} at a current density of 1,000 mA g^{-1}. Vanadium dissolution was observed, resulting in a poor cyclability of the material. Olivine $FePO_4$/C composite, obtained after delithiating $LiFePO_4$, amounted to a discharge capacity of 118 mA h g^{-1} at a scan rate of 10 mV s^{-1} in saturated $NaNO_3$ solution.[92] Using potentiodynamic polarization, $LiFePO_4$ was transformed entirely to $NaFePO_4$. $NaFePO_4$ was tested in 1 M Na_2SO_4 electrolyte, and a capacity of 70 mA h g^{-1} at C/5 rate was obtained at room temperature.[93] While at 55 °C, the polarization was reduced to a great extent and a discharge capacity of 110 mA h g^{-1} was obtained at C/10 rate. A 0.6 V full cell was assembled with NTP anode and a discharge capacity of 70 mA h g^{-1} was obtained with 76% capacity retention after 20 cycles. By employing CV, Minakshi *et al.* showed reversible sodium (de)intercalation in *maricite* $NaMn_{1/3}Co_{1/3}Ni_{1/3}PO_4$ in 7 M NaOH solution.[94] The electrochemical

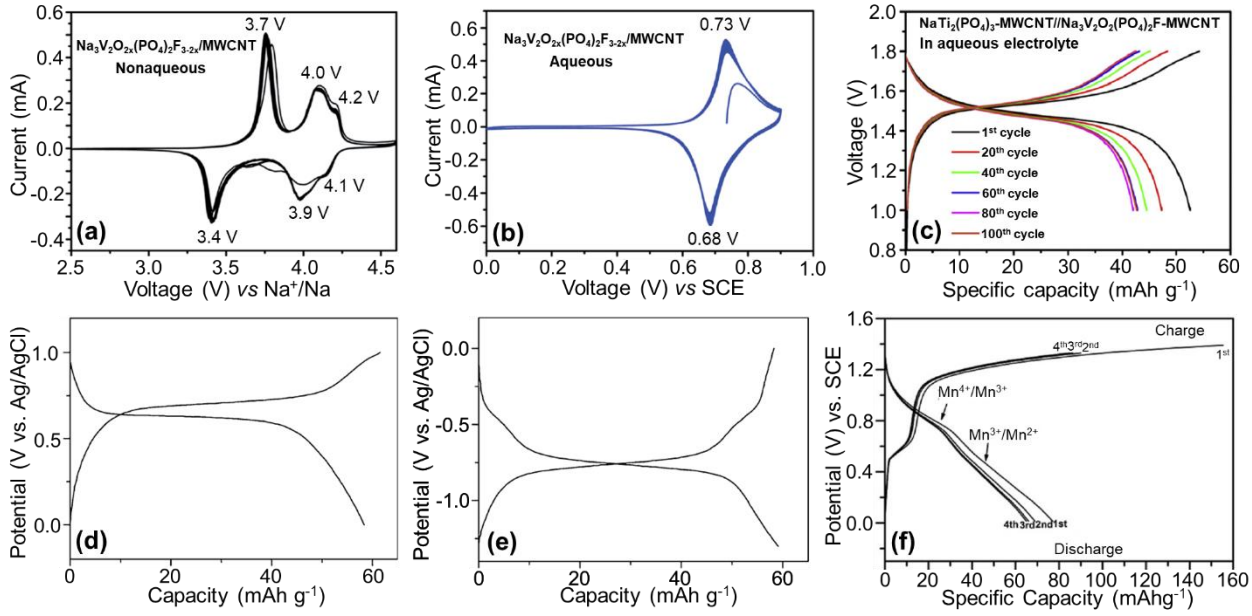

Fig. 6 (a, b) CV of $Na_3V_2O_{2x}(PO_4)_2F_{3-2x}$-MWCNT composite in non-aqueous and 10 M $NaClO_4$ aqueous electrolyte, recorded at a scan rate of 0.2 mA s^{-1}. (c) (Dis)charge curves of NTP-MWCNT//$Na_3V_2O_2(PO_4)_2F$-MWCNT full-cell in 10 M $NaClO_4$ + 2% VC electrolyte at 1C rate. (d) (Dis)charge curve of $Na_3MnTi(PO_4)_3$ at C/2 rate when cycled between 0.0 and 1.0 V vs. Ag/AgCl in 1 M Na_2SO_4 electrolyte. (e) (Dis)charge curve of $Na_3MnTi(PO_4)_3$ at C/2 rate when cycled between -1.3 and 0.0 V vs. Ag/AgCl in 1 M Na_2SO_4 electrolyte. (f) Electrochemical performance of $Na_3MnCO_3PO_4$//NTP cell in 5 M $NaNO_3$ aqueous electrolyte at C/5 rate. (a, b) Reproduced with permission from ref 78. Copyright 2015 The Royal Society of Chemistry. (c) Reproduced with permission from ref 80. Copyright 2016 Elsevier. (d, e) Reproduced with permission from ref 85. Copyright 2016 Wiley-VCH. (f) Reproduced with permission from ref 88. Copyright 2020 Elsevier.

performances of the polyanionic cathode materials for ASIB applications are summarized in Table 3.

5. Polyanionic cathode materials for aqueous zinc-ion batteries (AZIB)

Since the first report on aqueous electrolytes for LIBs by Dahn *et al.*, many materials have been explored as cathodes, e.g., $LiCoO_2$, $LiFePO_4$, $LiMn_2O_4$, *etc.*[45,95–99] However, the insufficient lithium reserves may make it challenging to implement aqueous LIBs for grid storage technologies. This led to the development of aqueous SIBs as a low-cost and environmentally benign energy storage technology where materials like $NaMnO_2$, $Na_2FeP_2O_7$, $Na_3V_2(PO_4)_3$, $NaFePO_4$, *etc.* were studied as cathodes.[66,83,93,100] However, the energy density delivered by ASIB is less than ALIB owing to the large ionic radius and high molecular weight of Na^+ as compared to Li^+. For multivalent-ion insertion, the strong electrostatic repulsion between the host lattice and multivalent ions pose some challenges.[101,102] In the case of aqueous magnesium-ion batteries, the development is hampered due to the lack of suitable cathodes as the kinetics of Mg^{2+} ions are very sluggish in the bulk host material.[103,104] Moreover, the unstable nature of magnesium-metal in aqueous media due to the formation of a passivation layer further cripples the kinetics of Mg^{2+} ions.[23] Aluminum-ion batteries exhibit high volumetric and gravimetric energy densities. However, the rapid formation of Al_2O_3 protection layer on aluminum-metal in aqueous media has hampered its promise. Moreover, the lack of suitable electrolytes results in a decay of cell efficiency and potential in magnesium-ion and aluminum-ion batteries. While the development of aqueous magnesium- and aluminum-ion batteries is plagued by the unstable nature of the corresponding metal anodes in water, the same is not true for zinc. Zinc-metal exhibits good electrochemical stability in aqueous media, owing to the high overpotential of the H_2 evolution reaction. It has a high abundance in the earth's crust, low redox potential (-0.76 V vs. SHE), and high theoretical capacity.[23–25] The high volumetric and gravimetric energy densities of zinc and the involvement of two electrons per ion in the redox reaction have made zinc-ion batteries an ideal alternative for grid-storage applications. Hence, reports on zinc-ion batteries with organic and aqueous electrolytes have increased drastically in the past few years.[105,106]

Metallic zinc is considered an ideal anode due to its high abundance, low cost, and long cycle life.[107] The use of zinc-metal anode dates back to 1799, when Volta *et al.* employed it in a voltaic cell. Since then, it has been used as an anode in primary and secondary batteries. Among all of them, alkaline Zn-MnO_2 has shown massive potential as a primary battery and still exists in the commercial market.[108] Many efforts were made to make rechargeable alkaline Zn-MnO_2 batteries, but the dendrite formation at the zinc-metal anode led to poor discharge performance and cycling life.[109,110] However, these issues can be circumvented using neutral pH-based aqueous electrolytes and high concentration electrolytes.[111] Utilizing this concept, Shoji *et al.* first reported a Zn-

Table 3. Overview of the electrochemical performances of polyanionic cathode materials for aqueous sodium-ion batteries.

Material/System	Electrolyte	Capacity/ mA h g^{-1} (C-rate)	% Capacity retention (cycle number)	Voltage (Energy density)	Ref
$Na_3V_2(PO_4)_3$	1 M Na_2SO_4	52 (8.5 C)	-	-	66
$Na_3V_2(PO_4)_3$/C	1 M Na_2SO_4	94.5 (10 C)	-	-	67
NTP//$Na_3V_2(PO_4)_3$	1 M Na_2SO_4	73 (3 A g^{-1})	50 (50) @10 A g^{-1}	1.2 V (36 W h kg^{-1})	68
Zn//$Na_3V_2(PO_4)_3$/C	0.5 M CH_3COONa/ $Zn(CH_3COO)_2$	93 (0.5 C)	77 (200) (0.5 C)	1.42 V (112 W h kg^{-1})	69
$Na_2VTi(PO_4)_3$@C	1 M Na_2SO_4	55 (0.5 C)	83 (600) @40 and 4 C	1.16 V (34 W h kg^{-1})	73
$Na_2VTi(PO_4)_3$ // $Na_2VTi(PO_4)_3$	1 M Na_2SO_4	50 (1 C)	70 (1000) @10 C	1.2 V (30 W h kg^{-1})	74
$Na_2VTi(PO_4)_3$/C // $Na_2VTi(PO_4)_3$/C	9.2 m $NaCF_3SO_3$	45 (0.2 C)	99 (1000) @20 C	1.2 V	75
Polyimide//$NaVPO_4F$	5 M $NaNO_3$	40 (50 mA g^{-1})	-	-	77
Zn // $Na_3V_2O_{2x}(PO_4)_2F_{3-2x}$-MWCNT	10 M $NaClO_4$	54 (1 C)	85 (400) @1 C	1.7 V (84 W h kg^{-1})	78
NTP//$Na_3V_2O_{2x}(PO_4)_2F_{3-2x}$-MWCNT	10 M $NaClO_4$ + 2 v% VC	39 (10 C)	85 (200) @10 C	1.5 V	79
NTP-MWCNT // $Na_3V_2O_2(PO_4)_2F$-MWCNT	10 M $NaClO_4$ + 2 v% VC	52.5 (1 C)	80 (100) @1 C	1.5 V	80
$Na_3V_2(PO_4)_2F_3$-SWCNT	17 m $NaClO_4$	81.3 (1 C)	71 (60) @1 C	-	81
$Na_3MnTi(PO_4)_3$ // $Na_3MnTi(PO_4)_3$	1 M Na_2SO_4	57.9 (0.5 C)	98 (100) @1 C	1.4 V (40 W h kg^{-1})	85
NTP-MWCNT // $Na_4MnV(PO_4)_3$-rGO	10 M $NaClO_4$ + 2 v% VC	97 (10 C)	52 (60) @10 C	1.3 V (130 W h kg^{-1})	86
NTP//$Na_3MnCO_3PO_4$	5 M $NaNO_3$	77.09 (C/5)	89 (100) @0.2 C	-	88
$Na_7V_4(P_2O_7)_4(PO_4)$/C	1 M Na_2SO_4	51 (80 mA g^{-1})	82 (50) @1000	-	91

* NTP = $NaTi_2(PO_4)_3$; Ref = Reference; MWCNT = Multi walled carbon nano tube;SWCNT = single walled carbon nano tube

MnO_2 aqueous battery using a mild acidic electrolyte, and this report opened the avenue for the field of aqueous ZIBs.[112] However, it is imperative to understand that in a highly acidic environment, protons can intercalate into the material instead of Zn^{2+} ions.[113] The aqueous ZIBs suffer due to a lack of proper cathode materials owing to the strong electrostatic interactions between divalent Zn^{2+} ion and the host, resulting in poor cycle life and slow kinetics.[23]

There have been many reports on rechargeable binary-ion batteries during last decade where a lithium insertion host was used as a cathode, zinc-metal as an anode, and lithium- and zinc-ion based binary solution was used an electrolyte. However, due to the high lithium cost, it is difficult for lithium-intercalation compounds to be used for AZIB applications.[23] Hence, sodium-based cathodes were explored. However, the quest for finding a suitable low-cost insertion material is still on, and few polyanionic materials have been reported. NASICON-type $M_3V_2(PO_4)_3$ (M = Na, Li) have gained most of the attraction for multivalent-ion insertion due to their thermodynamically stable structural framework. It has been observed that vanadium phosphate materials degrade in most of the aqueous electrolytes after a few cycles, but ion substitution can suppress cathode dissolution. The electrochemical performance of titanium substituted $Na_3V_2(PO_4)_3$ was studied in 1 M $Zn(NO_3)_2$, and a discharge capacity of more than 50 mA h g^{-1} with ~ 93% capacity retention after ten cycles was reported at 2C rate (Fig. 7a).[72]

Li *et al.* reported graphene-like carbon wrapped $Na_3V_2(PO_4)_3$ as a cathode for AZIB with 0.5 M $Zn(CH_3COO)_2$ electrolyte.[114] During the first charge, they deintercalated two Na-

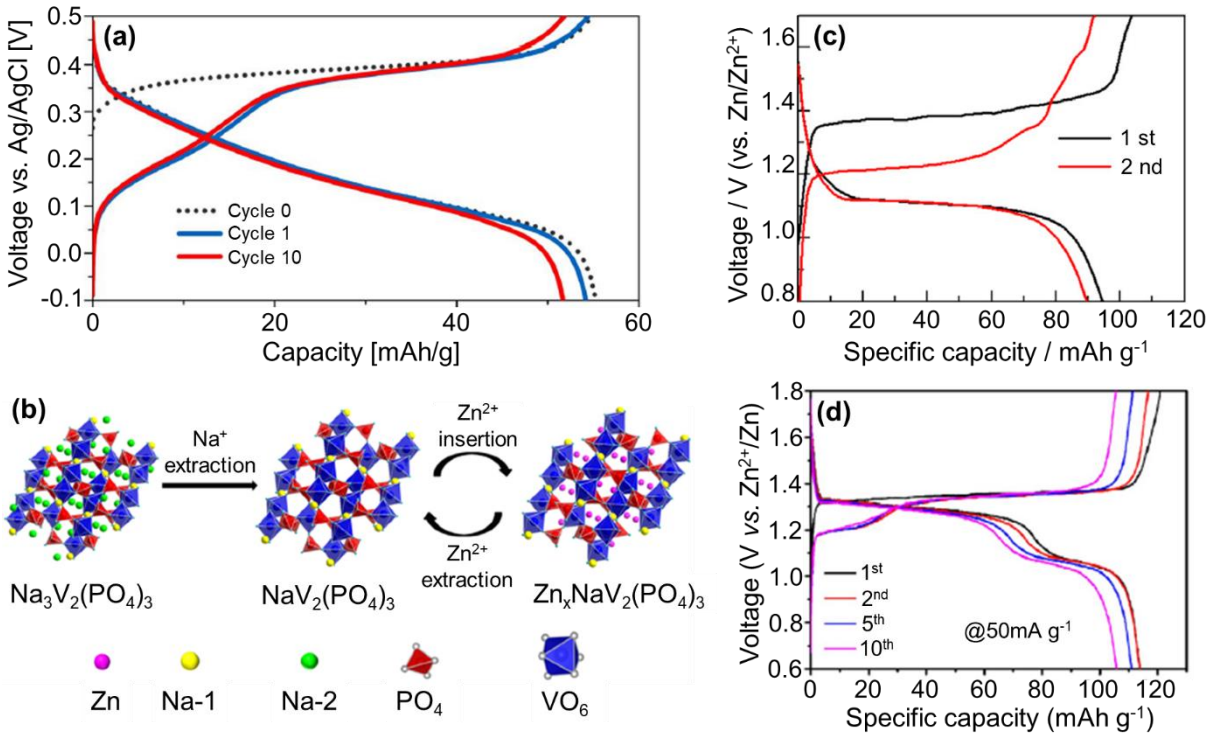

Fig. 7 (a) (Dis)charge profiles of $Na_2TiV(PO_4)_3$ at 2C rate in 1 M $Zn(NO_3)_2$ electrolyte. (b) Schematic representation of phase/structural transition in $Na_3V_2(PO_4)_3$ during Zn-insertion. (c) Galvanostatic (dis)charge curves of a Zn | 0.5 M $Zn(CH_3COO)_2$ | $Na_3V_2(PO_4)_3$ cell at C/2 rate. (d) Electrochemical performance of $Na_3V_2(PO_4)_3$@rGO at 50 mA g^{-1} when cycled in the potential window of 0.6-1.8 V vs. Zn^{2+}/Zn in 2 M $Zn(CF_3SO_3)_2$ aqueous electrolyte. (a) Reproduced with permission from ref 72. Copyright 2015 The Electrochemical Society. (b, c) Reproduced with permission from ref 114. Copyright 2016 Elsevier. (d) Reproduced with permission from ref 115. Copyright 2019 Elsevier.

ions from $Na_3V_2(PO_4)_3$. During subsequent discharge, Zn^{2+} ions were intercalated into the structure, which was confirmed by the significant potential difference between the first and second discharge plateaus (Fig. 7b). This was attributed to the chemical potential difference between $Na_3V_2(PO_4)_3$ and $Zn_xNaV_2(PO_4)_3$, which also meant that the redox potential of the zinc intercalated phase is lower than the pristine phase. When cycled between a potential window of 0.8 to 1.7 V vs. Zn/Zn^{2+}, the material delivered a discharge capacity of 97 mA h g^{-1} at C/2 rate and 74% of the capacity was retained after 100 cycles (Fig. 7c). From *ex-situ* XRD, they found that the Zn-intercalated phase also adopts the NASICON-type structure, and an ion occupancy variation mechanism was proposed. At the completely charged state, the peaks were attributed to desodiated $NaV_2(PO_4)_3$ phase while during discharge, an emergence of second phase at the expense of $NaV_2(PO_4)_3$ was observed. The phase obtained at end of discharge was neither $Na_3V_2(PO_4)_3$ nor $NaV_2(PO_4)_3$, but the peaks belonged to the NASICON structure. However, the same group tested this material in a binary electrolyte where they used 0.5 M $CH_3COONa/Zn(CH_3COO)_2$ and observed only Na-ion (de)intercalation.[69] In binary electrolytes, Li^+ or Na^+ suppresses the intercalation of Zn^{2+} ions. The underlying reasons behind this suppression are still unknown. However, Hu *et al.* first demonstrated Zn^{2+}/Na^+ co-insertion into rGO coated $Na_3V_2(PO_4)_3$ in 2 M $Zn(CF_3SO_3)_2$ electrolyte.[115] It delivered a discharge capacity of 114 mA h g^{-1} at a current density of 50 mA g^{-1} with good long-term cyclability and rate capability (Fig. 7d). Wang's group made an effort to understand the role of water in improving the kinetics of bivalent ion diffusion (especially Zn^{2+} ion diffusion) by using layered $VOPO_4$ and its hydrates as a model cathode material.[116] They observed that the presence of water molecules at the electrode/electrolyte interface assists in Zn^{2+} ions diffusion while the structural water helps alter the working potential. They found that during (dis)charge, a dynamic equilibrium between the electrode and bulk electrolyte is established, which plays a vital role in the electrochemical performance.

Li *et al.* first reported a fluorophosphate-based $Na_3V_2(PO_4)_2F_3$ cathode.[117] To minimize dendrite formation, they used a carbon film-coated zinc-metal anode. They obtained a 1.62 V cell with an energy density of 98 W h kg^{-1}. On a bare zinc-metal anode, the dendrite growth occurred vertically, resulting in poor electrochemical performance. In a carbon film-coated zinc-metal anode, the dendrite growth occurred horizontally and, hence, produced better performance. In the voltage window of 0.8 to 1.9 V vs. Zn/Zn^{2+}, the material delivered a discharge capacity of 65 mA h g^{-1}, corresponding to 0.5 Zn-insertion at a current density of 0.08 A g^{-1} (Fig. 8a). At 1 A g^{-1}, the material delivered a discharge capacity of 46 mA h g^{-1}, 95% of which was retained after 4,000 cycles (Fig. 8b). Our group recently studied the storage mechanism inside $Na_3V_2(PO_4)_2F_3$ in both aqueous and non-aqueous electrolytes.[118] In the case of

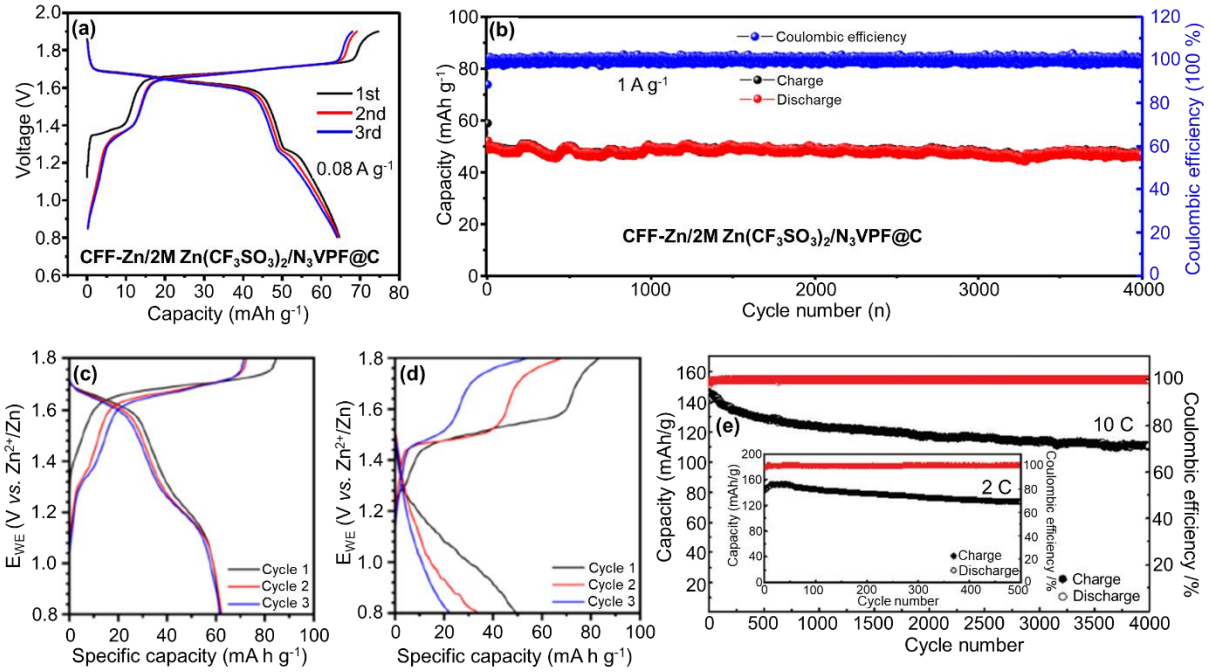

Fig. 8 (a) First three (dis)charge profiles of $Na_3V_2(PO_4)_2F_3$@C at 0.08 A g^{-1} in 2 M $Zn(CF_3SO_3)_2$ electrolyte. (b) Cyclability of $Na_3V_2(PO_4)_2F_3$@C at 1 A g^{-1} up to 4,000 cycles. (c) Electrochemical performance of $Na_3V_2(PO_4)_2F_3$/C at 1C rate in 3 M $Zn(CF_3SO_3)_2$ aqueous electrolyte. (d) Electrochemical performance of $Na_3V_2(PO_4)_2F_3$/C at C/3 rate in 0.3 M $Zn(CF_3SO_3)_2$ in acetonitrile non-aqueous electrolyte. (e) Cycling performance and coulombic efficiency of $LiV_2(PO_4)_3$ at 10C and 2C rates, respectively, up to 4000 and 500 cycles in 4 m $Zn(OTf)_2$ as an electrolyte. (a, b) Reproduced with permission from ref 117. Copyright 2018 Elsevier. (c, d) Reproduced with permission from ref 118. Copyright 2020 American Chemical Society. (e) Reproduced with permission from ref 119. Copyright 2018 The Royal Society of Chemistry.

aqueous electrolytes, at 1C rate, the cell delivered a discharge capacity of 61 mA h g^{-1} with good cycling stability for ten cycles (Fig. 8c). However, in the case of non-aqueous electrolytes, even at a C/3 rate, a discharge capacity of 49 mA h g^{-1} was obtained, which faded to 11 mA h g^{-1} after ten cycles (Fig. 8d). The *ex-situ* XRD and energy dispersive X-ray spectroscopy (EDX) analysis showed that in non-aqueous electrolyte, after the removal of Na-ions from the host lattice during first charge, Zn^{2+} and Na^+ co-insertion occurred during the subsequent discharge. Moreover, during the first discharge, more Na^+ ions were inserted back into the material. However, with gradual cycling, it changed to only Zn^{2+} insertion as the electrolyte is Zn-based, and Na^+ ions were scattered in the bulk of the electrolyte after a few cycles. Due to strong electrostatic interactions between Zn^{2+} and the host, intercalation kinetics was sluggish, hence poor cyclability was observed. Whereas, in the case of aqueous electrolyte, the EDX analysis of the discharged sample showed no peaks for Zn-ions, implying that Zn-ions are not responsible for the discharge capacity. We inferred that it is proton insertion that is responsible for the electrochemical activity, although EDX analysis after ten cycles did show a small amount of Zn^{2+} ions intercalated into the structure.

Wang's group reported $LiV_2(PO_4)_3$ as a high power density (8,000 W kg^{-1}) and high energy density (218 W h kg^{-1}) cathode for aqueous ZIBs with 4 m zinc trifluoromethanesulfonate ($Zn(OTf)_2$) as an electrolyte.[119] The host for Zn-ion insertion was obtained electrochemically by removing two lithium ions from $Li_3V_2(PO_4)_3$. The electronic structure of $LiV_2(PO_4)_3$ obtained by the density of states (DOS) showed *p-d* hybridization of V-*d* and O-*p* bands. This meant that the electrons introduced upon Zn-intercalation are accommodated nicely by both V and O sites, which resulted in much better kinetics of Zn^{2+} ions inside the host lattice. On cycling between 0.2 - 1.9 V vs. Zn/Zn^{2+}, a discharge capacity of 141 mA h g^{-1} was obtained at 2C rate with an average discharge potential of 1.3 V. The material exhibited excellent cycling stability with capacity decay rates of 0.028 % and 0.0053 %, respectively, at 2C rate for 500 cycles and 10C rate for 4,000 cycles (Fig. 8e). From *in-operando* XRD analysis, they reported the presence of both solid-solution and two-phase transition during cycling. The fast kinetics of Zn^{2+} ions were even maintained at a low temperature of -20 °C, where 75.8% of the room temperature capacity was retained at 2C rate.

Wan *et al.* utilized oxygen anionic redox to enhance the energy density of $VOPO_4$ || Zn based battery by employing a highly concentrated 21 m $LiN(CF_3SO_2)_2$ + 1 m $Zn(CF_3SO_3)_2$ electrolyte.[120] The average voltage was enhanced to 1.56 V, and after 1,000 cycles, a capacity of 74 mA h g^{-1} was obtained at 1 A g^{-1}, corresponding to 93% retention. Sun *et al.* reported $VOPO_4.xH_2O$ as a cathode, and they observed that the material decomposed into VO_x in conventional $Zn(OTf)_2$ electrolyte, hence, leading to poor cyclability.[121] They also observed the formation of a phosphate-based impurity upon decomposition. They used a highly concentrated electrolyte (13 m $ZnCl_2$) with a phosphate-based additive (0.8 m H_3PO_4) to circumvent this issue. By using the additive, the equilibrium was shifted toward

Table 4. Overview of the electrochemical performances of polyanionic cathode materials for aqueous zinc-ion batteries.

Material/System	Electrolyte	Capacity/ mA h g^{-1} (C-rate)	% Capacity retention (cycle number)	Voltage (Energy density)	Ref
$Na_3V_2(PO_4)_3$	1 M $Zn(NO_3)_2$	>50 (2 C)	-	-	72
$Na_3V_2(PO_4)_3$/C	0.5 M $Zn(CH_3COO)_2$	97 (0.5 C)	74 (100) @0.5 C	~ 1.1 V	114
$Na_3V_2(PO_4)_3$@rGO	2 M $Zn(CF_3SO_3)_2$	114 (50 mA g^{-1})	75 (200) @500 mA g^{-1}	~ 1.23 V	115
$Na_3V_2(PO_4)_2F_3$	2 M $Zn(CF_3SO_3)_2$	64.7 (0.08 A g^{-1})	95 (4000) @1 A g^{-1}	1.62 V (97.5 W h kg^{-1})	117
$Na_3V_2(PO_4)_2F_3$/C	3 M $Zn(CF_3SO_3)_2$	61 (1 C)	-	-	118
$LiV_2(PO_4)_3$@C	4 m $Zn(OTf)_2$	141 (2 C)	86 (500) @2 C	1.3 V (183 W h kg^{-1})	119
$VOPO_4$	21 m LiTFSI + 1 m $Zn(OTf)_2$	139 (0.05 A g^{-1})	93 (1000) @1 A g^{-1}	1.56 V (217 W h kg^{-1})	120
$VOPO_4.xH_2O$	13 m $ZnCl_2$ + 0.8 m H_3PO_4	170 (0.1 A g^{-1})	-	1.35 V (230 W h kg^{-1})	121
$Na_3V_2(PO_4)_2O_{1.6}F_{1.4}$	25 m $ZnCl_2$ + 5 m NH_4Cl	155 (50 mA g^{-1})	74 (7000) @2 A g^{-1}	1.46 V	122
VPO_4F	1 M $ZnSO_4$	~ 120 (C/20)	-	~ 1.5 V	123
$Mn_{0.25}(VO)_{0.75}PO_4.2.25H_2O$	3 M $Zn(CF_3SO_3)_2$	208 (0.1 A g^{-1})	88 (700) @5 A g^{-1}	0.95 V (198 W h kg^{-1})	139

* LiTFSI = $LiN(CF_3SO_2)_2$; $Zn(OTf)_2$ = $Zn(CF_3SO_3)_2$; Ref = Reference

the back direction and, hence, minimized the decomposition. They reported a discharge capacity of 170 mA h g^{-1} with good capacity retention after 500 cycles. Recently, Ni *et al.* employed a neutral *water-in-bisalt* based electrolyte comprising 25 m $ZnCl_2$ + 5 m NH_4Cl and reported a rGO wrapped $Na_3V_2(PO_4)_2O_{1.6}F_{1.4}$ as a cathode.[122] The material delivered a high specific capacity of 155 mA h g^{-1} at a current of 50 mA g^{-1}. It exhibited a high working potential of 1.46 V when cycled in the potential window of 0.4 to 2.1 V vs. Zn/Zn^{2+}. They initially tested the material in 30 m $ZnCl_2$ electrolyte but observed a severe capacity fading, which was improved when they adopted a *water-in-bisalt* type electrolyte configuration. This was attributed to the pH-neutral electrolyte, which is less corrosive, assisting in enhancing the battery performance. At a high current rate of 2 A g^{-1}, the cell delivered a capacity of 83 mA h g^{-1}, 73.5% of which was retained after 7,000 cycles. This is the best performance reported to date among polyanionic cathode materials for AZIB. They tried to understand further the structural evolution with *ex-situ* X-ray diffraction. They reported structural reversibility during (dis)charge and observed minor proton insertion electrochemically with *ex-situ* XRD. Our group did subsequent research on multivalent-ion batteries, especially AZIB. In 2020, we reported delithiated *tavorite*-based VPO_4F as a cathode for both aqueous and non-aqueous ZIBs.[123] We also observed that proton insertion leads to structural instability and that zinc insertion is not favorable even when a highly concentrated electrolyte is used. With a considerable amount of work done on polyanionic hosts for aqueous ZIBs in the last decade, they exhibit a bright future for energy storage. However, careful analysis must be carried out both electrochemically and structurally to understand the insertion mechanisms. The electrochemical performances of the polyanionic cathode materials for AZIB applications are summarized in Table 4.

6. Challenges and outlook

Aqueous batteries have emerged as an attractive domain from a sustainability and safety points of view. Moreover, shifting to aqueous electrolytes imparts a positive impact on the environment and reduces the overall cost of batteries. However, there remains many challenges for the practical application of these batteries, especially for grid-storage applications.[124] Some of these challenges are listed below:

1. *Narrow-voltage window*: While the operating mechanism of aqueous electrolytes is similar to that of non-aqueous electrolytes, they exhibit a narrower operating potential window of < 2 V much less than that of organic electrolytes stemming from the inherent thermodynamic potential of water. This is a major challenge, which restricts the full utilization of the cathode material, resulting in lower

energy density than organic electrolytes. Cycling beyond this voltage window range will result in H_2/O_2 evolution via two half-reactions, *viz.,* the oxygen evolution reaction (OER) and hydrogen evolution reaction (HER). The mechanism of OER and HER involve, respectively, four and two electron transfer and the overall chemical reactions are represented by equations (1-4).

OER: $2H_2O \rightarrow O_2 + 4H^+ + 4e^-$ (in acidic conditions) (1)

OER: $4OH^- \rightarrow O_2 + 2H_2O + 4e^-$ (in alkaline conditions) (2)

HER: $2H^+ + 2e^- \rightarrow H_2$ (in acidic conditions) (3)

HER: $2H_2O + 2e^- \rightarrow H_2 + 2OH^-$ (in alkaline conditions) (4)

These reactions are sensitive to pH and the surface of the material. Moreover, side reactions like proton consumption due to HER/OER can also occur during long-term cycling. Many high-voltage cathode materials exhibit (de)intercalation potentials, which lie outside the stable voltage window of aqueous electrolytes. This demands either a careful selection of cathode materials or a widening of the potential window. Moreover, the cathodes should not exhibit any electrocatalytic properties, e.g., $Li_2MnP_2O_7$, which is reported as a water oxidation catalysts.[125]

2. *Cathode dissolution*: Many materials, especially vanadium-based, are unstable in aqueous electrolytes. Vanadium dissolution is favored in mildly acidic electrolytes and results in a decay of electrochemical performance. This dissolution results in a loss of active material, which tends to deposit on the anode leading to the formation of a passivation layer. This is commonly observed in aqueous zinc-ion batteries.[24] In them, it has been observed that the vanadium-dissolution rate is high at slower C-rates and low at higher C-rates. It is one of the reasons for poor long-term cyclability. There is currently no effective way to completely prevent vanadium dissolution, but it can be lessened by using materials that exhibit more stable V-O bonds. This can be achieved by either doping or by anion substitution. Titanium doped $Na_3V_2(PO_4)_3$ is a classic example of high structural stability in aqueous electrolyte compared to the undoped material.[72] The pH of the electrolyte also results in material dissolution, e.g., $LiFePO_4$ decomposing into Fe_3O_4 under alkaline conditions.[40] Hence, effect of pH on structural stability must be studied carefully before testing the electrochemical performance. The use of surface coatings or surface stabilizers is a possible way to circumvent cathode dissolution.

3. *Electrostatic interactions*: Aqueous zinc-ion batteries do offer a possibility of achieving high energy density owing to two-electron transfer due to divalent Zn^{2+} ions. However, the high charge density leads to high electrostatic interactions between the intercalated ion and the host. This results in structural expansion of the lattice, triggering a possible structural distortion/collapse during continuous cycling. These electrostatic interactions also result in slow kinetics of Zn^{2+} ions inside the host and/or low electrochemical utilization and reversible capacity. Phase transitions (e.g., $Zn_3V_2O_7(OH)_2.2H_2O$) can also occur at a critical amount of zinc, which can have a detrimental effect on the electrochemical performance.[126] This issue can be circumvented by selecting materials with high structural stability and flexible ion diffusion channels. The diffusion pathways can be broadened by either doping or by taking materials with crystal water.

4. *Dendrite growth*: Apart from AZIB, metals cannot be used as anode in other metal-ion aqueous batteries. Hence, the dendrite issue is more pronounced in AZIB, stemming from repeated plating and stripping of zinc. The activity and solubility of zinc is high in alkaline electrolytes (Zn-air, Zn-Mn, *etc.*), resulting in a rapid formation of dendrites as compared to acidic or near neutral electrolytes. Although the process of zinc plating and stripping is inevitable, it can be reduced to some extent by using mild pH based aqueous electrolytes.

5. *Byproduct formation and proton co-insertion*: Continuous cycling also results in the formation of some byproducts. In AZIB, $Zn_4(SO_4)(OH)_6.nH_2O$ byproduct formation is a commonly observed phenomenon.[127] There is no known mechanism to explain such byproduct formation, but it can result from side reactions between dissolved oxygen and the ions present in the electrolyte.[128] These byproducts can accumulate at the interface and can affect the electrochemical performance by increasing the charge-transfer resistance. Electrodes with porous morphology can assist in accommodating the byproducts and providing more reaction sites for the intercalating ions. Use of suitable additives and removal of dissolved oxygen from the electrolyte can further reduce side reactions and enhance the electrochemical performance. Proton co-insertion is a commonly observed phenomenon in aqueous batteries, especially in acidic electrolytes. One way to avoid this problem is the use of alkaline electrolytes, but it is observed that many materials are not stable in high pH electrolytes. Hence, use of highly concentrated WISE is preferred.

Although polyanionic materials are touted as one of the promising candidates for aqueous batteries, there are issues, which need to be addressed. While the oxide materials exhibit good electronic conductivity and high densities, which make them attractive for portable electronic devices and electric vehicles, polyanionic materials exhibit poor electronic conductivity and require further materials processing, resulting in additional cost and low tap density. The electronic conductivity can be improved by particle nano-sizing and carbon coating. Controlling the morphology can also help to improve the tap density. The polyanionic subunits are electrochemically inactive and bulky, so these materials exhibit low practical capacities. Some polyanionic materials that are studied extensively in aqueous electrolytes consist of precious and toxic metals, *i.e.*, vanadium. Hence, there is a need to replace them with economic and environmentally friendly elements. The redox potential of polyanionic materials can be tuned by using different polyanionic subunits. Coupling anions like F^- with $(PO_4)^{3-}$ can lead to cell voltages beyond 4.2 V (*e.g.*, Na_2CoPO_4F). However, application of such materials is further restricted in aqueous electrolytes due to their narrow operating voltage window.

Although commercialization of aqueous batteries faces some critical challenges, there are some possible future directions, which could prove vital for the development of the field. The researchers must emphasize a fundamental and in-depth understanding of the storage mechanisms in polyanionic host materials. Various *in-situ* characterization techniques, such as X-ray diffraction, Raman spectroscopy, and X-ray photoelectron spectroscopy must be implemented to understand precise structural changes, interface phenomena, and reaction mechanisms. Since the narrow operating voltage limits aqueous batteries, characterization techniques are further recommended. The morphological stability of the electrodes can be studied by scanning electron microscopy to improve the long-term cycling performance. The experimental observations must be complemented well by theoretical calculations like density functional method and molecular dynamics simulation *etc.*, for further understanding of reaction mechanisms.

Narrow operating voltage window is a major cause for low energy density and hinder the commercialization of aqueous batteries. With the inception of highly concentrated WISE and hydrate-melt electrolytes,[26,28] it is feasible to test high-voltage polyanionic cathode materials for aqueous batteries, as the operating voltage window can be enhanced to 3-4 V using such electrolytes. The amount of free water molecules in such high concentrated electrolytes is lower, which helps in impeding the electrochemical activity of water. They also help in building a solid-electrolyte interphase (SEI) layer at the anode by anion reduction. The first report on WISE utilized 21 m lithium bis(trifluoromethane)sulfonimide as a salt, but to overcome the saturation limit of the salt, different salts were reported for "water-in-bisalt" type electrolytes like lithium trifluoromethanesulfonate (LiOTf), lithium bis(pentafluoroethanesulfonyl)imide (LiBETI), *etc.*[26,27,129] But the salts generally used in such high-concentrated electrolytes are expensive and toxic with high viscosity and weight, making it challenging to use them at commercial scale. Concentrated mixed cation acetate WISE (32 m potassium acetate-8 m lithium acetate) and 'water-in-ionomer' gel (50% lithiated polyacrylic acid-50% H_2O) were reported to circumvent some of these issues.[130,131] Although the acetate-based electrolytes cannot form fluorinated SEI on the surface, the gel electrolytes have more water content, which can lead to a narrow voltage window and hence low energy density. Recently, by utilizing the concept of molecular crowding in living cells, a molecular crowding aqueous electrolyte was reported with a very low concentration of LiTFSI (2 m LiTFSI) and by utilizing poly(ethylene glycol) as a water-miscible polymer.[132] The electrolyte exhibited a stable potential window of 3.2 V with excellent HER stability. There is scope to test different additives and salts for aqueous electrolytes to make them economical and environmentally friendly.

It is well reported that O_2-free, concentrated, and high pH electrolytes are good for insertion-based materials. However, the overpotentials of HER and OER are large in neutral pH. It is necessary to understand the importance of pH for aqueous batteries. Hence, the electrochemical performance of polyanionic materials must be analysed in neutral electrolytes. pH fluctuations also occur during cycling, which might deteriorate the electrochemical performance. Additives like acetic acid has been reported as a buffer additive, resulting in improved long-term cycling performance.[133] Electrode designs must be optimized by surface coatings through atomic layer deposition, ion-doping, defects, or cation deficiencies, and artificial SEI to avoid cathode degradation. These techniques improve the kinetics of the intercalated species inside the host and enhance the structural stability of the cathode, resulting in better electrochemical performance. Capacity balancing is another crucial way to fully utilize the electrochemical stability window of aqueous electrolytes. Water decomposition and zinc dendrite growth are major contributors for poor cycling in AZIB. Electrolyte additives and surface engineering can help suppressing the dendrite formation and cation dissolution. Use of dimethyl sulfoxide (DMSO) in dilute aqueous electrolyte has been shown to suppress water reduction and dendrite growth. DMSO replaces H_2O in the Zn^{2+} solvation sheath due to its high Gutmann donor number, which inhibits the decomposition of water.[134] Moreover, the decomposition of DMSO solvation sphere led to $Zn_{12}(SO_4)_3Cl_3(OH)_{15}.5H_2O$, $ZnSO_3$, and ZnS based SEI, which prevents dendrite growth. *In-situ* formation of surface shielding layer has been shown to suppress manganese dissolution in Prussian blue analogue, leading to 83% retention after 6,500 cycles at a high current density.[135] Use of biphasic materials can also help in enhancing the performance owing to more active sites. A biphasic vanadate was reported for AZIB, delivering excellent rate capabilities owing to the interfacial adsorption-insertion mechanism induces by phase boundaries.[136] There are reports of solid and gel-based electrolytes for aqueous zinc-ion batteries, imparting flexible and stretchable characteristics to the battery.[24] This gives a new dimension for researchers to explore in the future, especially for aqueous lithium-ion batteries.

Fluorophosphate-based cathode materials have shown excellent structural stability in aqueous electrolytes. Due to toxicity associated with vanadium-based materials, other 3-d transition metal (M = Fe, Co, Mn) based fluorophosphates can also be explored using highly concentrated electrolytes. Fabricating full cells with fluorophosphates will yield a high operating voltage. Polyanionic materials is a rich class where many materials can be realized by substituting different polyanionic subunit and transition metal ions, *i.e.*, $A_xMM'(XO_4)_3$ (A = Li, Na and Zn; M and M' = transition- metal ion; X= Si, S, P, etc.). Among all the polyanionic subunits, $(PO_4)^{3-}$ offers the most variety of M and M' substitutions. Moreover, as compared to sulphates, borates, and silicates, synthesis of phosphate-based materials is straightforward with good yields. Hence, a lot of phosphate-based materials have been studied for aqueous battery applications. There is scope to explore other polyanionic chemistries for aqueous batteries application, *e.g.*, manganese silicate (Mn_2SiO_4) has been studied for AZIB applications.[137,138] Borate subunits are too bulky due to their high molecular weight and their low redox potentials make them unattractive for aqueous battery applications. Sulfate-based materials exhibit poor structural stability in water. But

with high-concentrated electrolytes having less water content, there exists an opportunity to test such polyanionic materials. Since polyanionic materials exhibit a variety of crystal structures, not all can be studied for aqueous battery applications. It is important to consider some factors like structural stability in water, high HER/OER potential, broad ion-diffusion pathways especially for Zn^{2+} migration, and multiple transition-metal oxidation states to tune the redox energies.

7. Summary

To summarize, aqueous electrolytes not only impart safety to the battery system, but they are also touted as the best alternatives to LIBs for stationary storage applications. The electrochemical performances of ALIB and ASIB were restricted due to limited choice of cathode materials and narrow operating potential window of the electrolytes. Conversely, AZIB based on near-neutral electrolytes have shown tremendous potential as indicated by the growing number of reports in the last five years owing to the efficient reversibility in Zn/Zn^{2+} plating and stripping. Moreover, the inception of WISE electrolytes in 2015 has augmented the research resulting in increased energy density and further fuelling the quest to find a suitable cathode material and in this pursuit, many oxide-based and polyanion-based materials have been reported. This review highlights some of the recent developments made in the field of polyanionic insertion materials for aqueous lithium, sodium, and zinc ion batteries. Not all polyanionic materials can be studied in aqueous electrolytes due to the constraint of a narrow operating potential window and structural stability. Hence, the number of reported articles in the literature is minimal as compared to organic electrolytes. However, many issues can be circumvented by using highly concentrated "*water-in-salt*" electrolytes, which enhance the redox potential window and improve the structural stability of materials in aqueous media. Since aqueous batteries are potential alternatives for energy storage technologies, particularly for grid storage, this review will benefit future and existing researchers working in this field.

Author contributions

LS did the literature survey, planned, and prepared the manuscript. AM supervised the work and edited the manuscript. All authors have given approval to the final version of the manuscript.

Conflicts of interest

The authors declare no conflict of interest.

Acknowledgements

This work was supported by the U.S. Department of Energy, Office of Basic Energy Sciences, Division of Materials Science and Engineering under award number DE-SC0005397 and Welch Foundation grant F-1254.

References

1 V. Etacheri, R. Marom, R. Elazari, G. Salitra and D. Aurbach, *Energy Environ. Sci.*, 2011, **4**, 3243–3262.
2 N. Nitta, F. Wu, J. T. Lee and G. Yushin, *Mater. Today*, 2015, **18**, 252–264.
3 D. Larcher and J.-M. Tarascon, *Nat. Chem.*, 2015, **7**, 19.
4 M. D. Slater, D. Kim, E. Lee and C. S. Johnson, *Adv. Funct. Mater.*, 2013, **23**, 947–958.
5 C. Vaalma, D. Buchholz, M. Weil and S. Passerini, *Nat. Rev. Mater.*, 2018, **3**, 18013.
6 N. Yabuuchi, K. Kubota, M. Dahbi and S. Komaba, *Chem. Rev.*, 2014, **114**, 11636–11682.
7 K. Kubota and S. Komaba, *J. Electrochem. Soc.*, 2015, **162**, A2538–A2550.
8 J.-Y. Hwang, S.-T. Myung and Y.-K. Sun, *Chem. Soc. Rev.*, 2017, **46**, 3529–3614.
9 C. Masquelier and L. Croguennec, *Chem. Rev.*, 2013, **113**, 6552–6591.
10 A. Manthiram, *Nat. Commun.*, 2020, **11**, 1550.
11 H. Kim, J. Hong, K.-Y. Park, H. Kim, S.-W. Kim and K. Kang, *Chem. Rev.*, 2014, **114**, 11788–11827.
12 F. Zheng, M. Kotobuki, S. Song, M. O. Lai and L. Lu, *J. Power Sources*, 2018, **389**, 198–213.
13 A. Manthiram and L. Li, *Adv. Energy Mater.*, 2015, **5**, 1401302.
14 Z. Khan, M. Vagin and X. Crispin, *Adv. Sci.*, 2020, **7**, 1902866.
15 X. Xu, K. San Hui, D. A. Dinh, K. N. Hui and H. Wang, *Mater. Horizons*, 2019, **6**, 1306–1335.
16 L. Li, S.-H. Chai, S. Dai and A. Manthiram, *Energy Environ. Sci.*, 2014, **7**, 2630–2636.
17 L. Sharma, R. Gond, B. Senthilkumar, A. Roy and P. Barpanda, *ACS Catal.*, 2019, **10**, 43-50.
18 W. Li, J. R. Dahn and D. S. Wainwright, *Science*, 1994, **264**, 1115–1118.
19 A. Eftekhari, *Adv. Energy Mater.*, 2018, **8**, 1801156.
20 J. Liu, C. Xu, Z. Chen, S. Ni and Z. X. Shen, *Green Energy Environ.*, 2018, **3**, 20–41.
21 W. Tang, Y. Zhu, Y. Hou, L. Liu, Y. Wu, K. P. Loh, H. Zhang and K. Zhu, *Energy Environ. Sci.*, 2013, **6**, 2093–2104.
22 M. Liu, H. Ao, Y. Jin, Z. Hou, X. Zhang, Y. Zhu and Y. Qian, *Mater. Today Energy*, 2020, **17**, 100432.
23 D. Selvakumaran, A. Pan, S. Liang and G. Cao, *J. Mater. Chem. A*, 2019, **7**, 18209–18236.
24 B. Tang, L. Shan, S. Liang and J. Zhou, *Energy Environ. Sci.*, 2019, **12**, 3288–3304.
25 G. Fang, J. Zhou, A. Pan and S. Liang, *ACS Energy Lett.*, 2018, **3**, 2480–2501.
26 Y. Yamada, K. Usui, K. Sodeyama, S. Ko, Y. Tateyama and A. Yamada, *Nat. Energy*, 2016, **1**, 16129.
27 L. Suo, O. Borodin, W. Sun, X. Fan, C. Yang, F. Wang, T. Gao, Z. Ma, M. Schroeder and A. von Cresce, *Angew. Chem. Int. Ed.*, 2016, **55**, 7136–7141.
28 L. Suo, O. Borodin, T. Gao, M. Olguin, J. Ho, X. Fan, C. Luo, C. Wang and K. Xu, *Science*, 2015, **350**, 938–943.

29 H. Zhang, X. Tan, H. Li, S. Passerini and W. Huang, *Energy Environ. Sci.*, 2021, **14**, 5788–5800.
30 M. S. WHITTINGHAM, *Science*, 1976, **192**, 1126–1127.
31 J. B. Goodenough and Y. Kim, *Chem. Mater.*, 2010, **22**, 587–603.
32 K. Mizushima, P. C. Jones, P. J. Wiseman and J. B. Goodenough, *Mater. Res. Bull.*, 1980, **15**, 783–789.
33 M. M. Thackeray, W. I. F. David, P. G. Bruce and J. B. Goodenough, *Mater. Res. Bull.*, 1983, **18**, 461–472.
34 A. Manthiram and J. B. Goodenough, *J. Solid State Chem.*, 1987, **71**, 349–360.
35 A. Manthiram and J. B. Goodenough, *J. Power Sources*, 1989, **26**, 403–408.
36 A. K. Padhi, K. S. Nanjundaswamy and J. B. Goodenough, *J. Electrochem. Soc.* , 1997, **144**, 1188–1194.
37 B. Senthilkumar, C. Murugesan, L. Sharma, S. Lochab and P. Barpanda, *Small Methods*, 2019, **3**, 1800253.
38 P. Barpanda, L. Lander, S. Nishimura and A. Yamada, *Adv. Energy Mater.*, 2018, **8**, 1703055.
39 L. Sharma, S. P. Adiga, H. N. Alshareef and P. Barpanda, *Adv. Energy Mater.*, 2020, **10**, 2001449.
40 M. Manickam, P. Singh, S. Thurgate and K. Prince, *J. Power Sources*, 2006, **158**, 646–649.
41 C. H. Mi, X. G. Zhang and H. L. Li, *J. Electroanal. Chem.*, 2007, **602**, 245–254.
42 P. He, X. Zhang, Y.-G. Wang, L. Cheng and Y.-Y. Xia, *J. Electrochem. Soc.*, 2007, **155**, A144.
43 F. Sauvage, J.-M. Tarascon and E. Baudrin, *Anal. Chim. Acta*, 2008, **622**, 163–168.
44 X.-H. Liu, T. Saito, T. Doi, S. Okada and J. Yamaki, *J. Power Sources*, 2009, **189**, 706–710.
45 J.-Y. Luo, W.-J. Cui, P. He and Y.-Y. Xia, *Nat. Chem.*, 2010, **2**, 760–765.
46 Y. Liu, C. Mi, C. Yuan and X. Zhang, *J. Electroanal. Chem.*, 2009, **628**, 73–80.
47 M. Zhao, B. Zhang, G. Huang, H. Zhang and X. Song, *J. Power Sources*, 2013, **232**, 181–186.
48 Y. Hou, X. Wang, Y. Zhu, C. Hu, Z. Chang, Y. Wu and R. Holze, *J. Mater. Chem. A*, 2013, **1**, 14713–14718.
49 W. Duan, M. Zhao, Y. Mizuta, Y. Li, T. Xu, F. Wang, T. Moriga and X. Song, *Phys. Chem. Chem. Phys.*, 2020, **22**, 1953–1962.
50 M. Minakshi, *Electrochim. Acta*, 2010, **55**, 9174–9178.
51 M. Minakshi, P. Singh, S. Thurgate and K. Prince, *Electrochem. Solid State Lett.*, 2006, **9**, A471.
52 M. Minakshi, A. Pandey, M. Blackford and M. Ionescu, *Energy & Fuels*, 2010, **24**, 6193–6197.
53 H. Manjunatha, T. V Venkatesha and G. S. Suresh, *J. Solid State Electrochem.*, 2012, **16**, 1941–1952.
54 M. Zhao, G. Huang, B. Zhang, F. Wang and X. Song, *J. Power Sources*, 2012, **211**, 202–207.
55 M. Zhao, G. Huang, W. Zhang, H. Zhang and X. Song, *Energy & Fuels*, 2013, **27**, 1162–1167.
56 M. Minakshi, P. Singh, N. Sharma, M. Blackford and M. Ionescu, *Ind. Eng. Chem. Res.*, 2011, **50**, 1899–1905.
57 M. Minakshi, P. Singh, D. Appadoo and D. E. Martin, *Electrochim. Acta*, 2011, **56**, 4356–4360.
58 M. Minakshi, N. Sharma, D. Ralph, D. Appadoo and K. Nallathamby, *Electrochem. Solid State Lett.*, 2011, **14**, A86.
59 J. Jiang, G. Tan, S. Peng, D. Qian, J. Liu, D. Luo and Y. Liu, *Electrochim. Acta*, 2013, **107**, 59–65.
60 Y. Lin, W. Wang, J. Zhang and C. Dai, *ECS Electrochem. Lett.*, 2014, **3**, A105.
61 H. Wang, H. Zhang, Y. Cheng, K. Feng, X. Li and H. Zhang, *Electrochim. Acta*, 2018, **278**, 279–289.
62 C. Yang, J. Chen, T. Qing, X. Fan, W. Sun, A. von Cresce, M. S. Ding, O. Borodin, J. Vatamanu and M. A. Schroeder, *Joule*, 2017, **1**, 122–132.
63 L. Sharma, K. Nakamoto, S. Okada and P. Barpanda, *J. Power Sources*, 2019, **429**, 17-21.
64 Z. Jian, L. Zhao, H. Pan, Y.-S. Hu, H. Li, W. Chen and L. Chen, *Electrochem. Commun.*, 2012, **14**, 86–89.
65 K. Saravanan, C. W. Mason, A. Rudola, K. H. Wong and P. Balaya, *Adv. Energy Mater.*, 2013, **3**, 444–450.
66 W. Song, X. Ji, Y. Zhu, H. Zhu, F. Li, J. Chen, F. Lu, Y. Yao and C. E. Banks, *ChemElectroChem*, 2014, **1**, 871–876.
67 L. Zhang, T. Huang and A. Yu, *J. Alloys Compd.*, 2015, **646**, 522–527.
68 Q. Zhang, C. Liao, T. Zhai and H. Li, *Electrochim. Acta*, 2016, **196**, 470–478.
69 G. Li, Z. Yang, Y. Jiang, W. Zhang and Y. Huang, *J. Power Sources*, 2016, **308**, 52–57.
70 T. Jin, X. Ji, P. Wang, K. Zhu, J. Zhang, L. Cao, L. Chen, C. Cui, T. Deng and S. Liu, *Angew. Chem. Int. Ed.*, 2021, **60**, 11943–11948.
71 H. Ao, C. Chen, Z. Hou, W. Cai, M. Liu, Y. Jin, X. Zhang, Y. Zhu and Y. Qian, *J. Mater. Chem. A*, 2020, **8**, 14190–14197.
72 C. W. Mason and F. Lange, *ECS Electrochem. Lett.*, 2015, **4**, A79.
73 J. Dong, G. Zhang, X. Wang, S. Zhang and C. Deng, *J. Mater. Chem. A*, 2017, **5**, 18725–18736.
74 H. Wang, T. Zhang, C. Chen, M. Ling, Z. Lin, S. Zhang, F. Pan and C. Liang, *Nano Res.*, 2018, **11**, 490–498.
75 H. Zhang, S. Jeong, B. Qin, D. Vieira Carvalho, D. Buchholz and S. Passerini, *ChemSusChem*, 2018, **11**, 1382–1389.
76 K. Nakamoto, R. Sakamoto, Y. Nishimura, J. Xia, M. Ito and S. Okada, *Electrochemistry*, 2021, 21–56.
77 H. Qin, Z. P. Song, H. Zhan and Y. H. Zhou, *J. Power Sources*, 2014, **249**, 367–372.
78 P. R. Kumar, Y. H. Jung, C. H. Lim and D. K. Kim, *J. Mater. Chem. A*, 2015, **3**, 6271–6275.
79 P. R. Kumar, Y. H. Jung, B. Moorthy and D. K. Kim, *J. Electrochem. Soc.*, 2016, **163**, A1484.
80 P. R. Kumar, Y. H. Jung, J. E. Wang and D. K. Kim, *J. Power Sources*, 2016, **324**, 421–427.
81 S. Liu, L. Wang, J. Liu, M. Zhou, Q. Nian, Y. Feng, Z. Tao and L. Shao, *J. Mater. Chem. A*, 2019, **7**, 248–256.
82 L. Sharma, K. Nakamoto, R. Sakamoto, S. Okada and P. Barpanda, *ChemElectroChem*, 2019, 6, 444-449.

83 Y. H. Jung, C. H. Lim, J.-H. Kim and D. K. Kim, *RSC Adv.*, 2014, **4**, 9799–9802.
84 K. Nakamoto, Y. Kano, A. Kitajou and S. Okada, *J. Power Sources*, 2016, **327**, 327–332.
85 H. Gao and J. B. Goodenough, *Angew. Chem. Int. Ed.*, 2016, **128**, 12960–12964.
86 P. R. Kumar, A. Kheireddine, U. Nisar, R. A. Shakoor, R. Essehli, R. Amin and I. Belharouak, *J. Power Sources*, 2019, **429**, 149–155.
87 B. Xie, R. Sakamoto, A. Kitajou, K. Nakamoto, L. Zhao, S. Okada, W. Kobayashi, M. Okada and T. Takahara, *Energies*, 2019, 12.
88 K. Shiprath, H. Manjunatha, K. C. B. Naidu, A. Khan, A. M. Asiri and R. Boddula, *Mater. Chem. Phys.*, 2020, **248**, 122952.
89 B. Xie, R. Sakamoto, A. Kitajou, K. Nakamoto, L. Zhao, S. Okada, Y. Fujita, N. Oka, T. Nishida, W. Kobayashi, M. Okada and T. Takahara, *Sci. Rep.*, 2020, **10**, 3278.
90 S. Kudekallu, H. Manjunatha, V. R. Kesamsetty and J. Sannapaneni, *J. Electrochem. Soc.*, 2021, **168**, 080523.
91 C. Deng, S. Zhang and Y. Wu, *Nanoscale*, 2015, **7**, 487–491.
92 M. Vujković and S. Mentus, *J. Power Sources*, 2014, **247**, 184–188.
93 A. J. Fernández-Ropero, D. Saurel, B. Acebedo, T. Rojo and M. Casas-Cabanas, *J. Power Sources*, 2015, **291**, 40–45.
94 M. Minakshi and D. Meyrick, *J. Alloys Compd.*, 2013, **555**, 10–15.
95 W. Tang, L. L. Liu, S. Tian, L. Li, Y. B. Yue, Y. P. Wu, S. Y. Guan and K. Zhu, *Electrochem. Commun.*, 2010, **12**, 1524–1526.
96 Q. Qu, L. Fu, X. Zhan, D. Samuelis, J. Maier, L. Li, S. Tian, Z. Li and Y. Wu, *Energy Environ. Sci.*, 2011, **4**, 3985–3990.
97 W. Tang, L. Liu, Y. Zhu, H. Sun, Y. Wu and K. Zhu, *Energy Environ. Sci.*, 2012, **5**, 6909–6913.
98 W. Tang, Y. Hou, F. Wang, L. Liu, Y. Wu and K. Zhu, *Nano Lett.*, 2013, **13**, 2036–2040.
99 X. Wang, Q. Qu, Y. Hou, F. Wang and Y. Wu, *Chem. Commun.*, 2013, **49**, 6179–6181.
100 Z. Hou, X. Li, J. Liang, Y. Zhu and Y. Qian, *J. Mater. Chem. A*, 2015, **3**, 1400–1404.
101 J. C. Knight, S. Therese and A. Manthiram, *J. Mater. Chem. A* 2015, **3**, 21077-21082.
102 J. C. Knight, S. Therese and A. Manthiram, *ACS Appl. Mater. Interfaces*, 2015, **7**, 22953–22961.
103 H. D. Yoo, I. Shterenberg, Y. Gofer, G. Gershinsky, N. Pour and D. Aurbach, *Energy Environ. Sci.*, 2013, **6**, 2265–2279.
104 I. Shterenberg, M. Salama, Y. Gofer, E. Levi and D. Aurbach, *MRS Bull.*, 2014, **39**, 453–460.
105 P. He, Q. Chen, M. Yan, X. Xu, L. Zhou, L. Mai and C.-W. Nan, *EnergyChem*, 2019, **1**, 100022.
106 J. Ming, J. Guo, C. Xia, W. Wang and H. N. Alshareef, *Mater. Sci. Eng. R Reports*, 2019, **135**, 58–84.
107 J. Lee, S. Tai Kim, R. Cao, N. Choi, M. Liu, K. T. Lee and J. Cho, *Adv. Energy Mater.*, 2011, **1**, 34–50.
108 M. Winter and R. J. Brodd, *Chem. Rev.*, 2004, **104**, 4245–4270.
109 X. Wang, F. Wang, L. Wang, M. Li, Y. Wang, B. Chen, Y. Zhu, L. Fu, L. Zha and L. Zhang, *Adv. Mater.*, 2016, **28**, 4904–4911.
110 P. Senguttuvan, S. Han, S. Kim, A. L. Lipson, S. Tepavcevic, T. T. Fister, I. D. Bloom, A. K. Burrell and C. S. Johnson, *Adv. Energy Mater.*, 2016, **6**, 1600826.
111 K. E. K. Sun, T. K. A. Hoang, T. N. L. Doan, Y. Yu, X. Zhu, Y. Tian and P. Chen, *ACS Appl. Mater. Interfaces*, 2017, **9**, 9681–9687.
112 T. Shoji, M. Hishinuma and T. Yamamoto, *J. Appl. Electrochem.*, 1988, **18**, 521–526.
113 W. Sun, F. Wang, S. Hou, C. Yang, X. Fan, Z. Ma, T. Gao, F. Han, R. Hu and M. Zhu, *J. Am. Chem. Soc.*, 2017, **139**, 9775–9778.
114 G. Li, Z. Yang, Y. Jiang, C. Jin, W. Huang, X. Ding and Y. Huang, *Nano Energy*, 2016, **25**, 211–217.
115 P. Hu, T. Zhu, X. Wang, X. Zhou, X. Wei, X. Yao, W. Luo, C. Shi, K. A. Owusu and L. Zhou, *Nano Energy*, 2019, **58**, 492–498.
116 F. Wang, W. Sun, Z. Shadike, E. Hu, X. Ji, T. Gao, X. Yang, K. Xu and C. Wang, *Angew. Chem. Int. Ed.*, 2018, **57**, 11978–11981.
117 W. Li, K. Wang, S. Cheng and K. Jiang, *Energy Storage Mater.*, 2018, **15**, 14–21.
118 M. J. Park and A. Manthiram, *ACS Appl. Energy Mater.*, 2020, **3**, 5015–5023.
119 F. Wang, E. Hu, W. Sun, T. Gao, X. Ji, X. Fan, F. Han, X.-Q. Yang, K. Xu and C. Wang, *Energy Environ. Sci.*, 2018, **11**, 3168–3175.
120 F. Wan, Y. Zhang, L. Zhang, D. Liu, C. Wang, L. Song, Z. Niu and J. Chen, *Angew. Chem. Int. Ed.*, 2019, **58**, 7062–7067.
121 H. Shi, Y. Song, Z. Qin, C. Li, D. Guo, X. Liu and X. Sun, *Angew. Chem. Int. Ed.*, 2019, **58**, 16057–16061.
122 Q. Ni, H. Jiang, S. Sandstrom, Y. Bai, H. Ren, X. Wu, Q. Guo, D. Yu, C. Wu and X. Ji, *Adv. Funct. Mater.*, 2020, **30**, 2003511.
123 H. Y. Asl, S. Sharma and A. Manthiram, *J. Mater. Chem. A*, 2020, **8**, 8262–8267.
124 D. Chao, W. Zhou, F. Xie, C. Ye, H. Li, M. Jaroniec and S.-Z. Qiao, *Sci. Adv.*, 2020, **6**, eaba4098.
125 J. Park, H. Kim, K. Jin, B. J. Lee, Y.-S. Park, H. Kim, I. Park, K. D. Yang, H.-Y. Jeong and J. Kim, *J. Am. Chem. Soc.*, 2014, **136**, 4201–4211.
126 B. Tang, G. Fang, J. Zhou, L. Wang, Y. Lei, C. Wang, T. Lin, Y. Tang and S. Liang, *Nano energy*, 2018, **51**, 579–587.
127 V. Soundharrajan, B. Sambandam, S. Kim, M. H. Alfaruqi, D. Y. Putro, J. Jo, S. Kim, V. Mathew, Y.-K. Sun and J. Kim, *Nano Lett.*, 2018, **18**, 2402–2410.
128 D. Kundu, S. H. Vajargah, L. Wan, B. Adams, D. Prendergast and L. F. Nazar, *Energy Environ. Sci.*, 2018, **11**, 881–892.
129 S. Ko, Y. Yamada, K. Miyazaki, T. Shimada, E. Watanabe, Y. Tateyama, T. Kamiya, T. Honda, J. Akikusa and A. Yamada, *Electrochem. Commun.*, 2019, **104**, 106488.
130 X. He, B. Yan, X. Zhang, Z. Liu, D. Bresser, J. Wang, R. Wang, X. Cao, Y. Su, H. Jia, C. P. Grey, H. Frielinghaus, D. G. Truhlar,

M. Winter, J. Li and E. Paillard, *Nat. Commun.*, 2018, **9**, 5320.

131 M. R. Lukatskaya, J. I. Feldblyum, D. G. Mackanic, F. Lissel, D. L. Michels, Y. Cui and Z. Bao, *Energy Environ. Sci.*, 2018, **11**, 2876–2883.

132 J. Xie, Z. Liang and Y. C. Lu, *Nat. Mater.*, 2020, **19**, 1006-1011.

133 Z. Liu, Y. Yang, S. Liang, B. Lu and J. Zhou, *Small Struc.*, 2021, **2**, 2100119.

134 L. Cao, D. Li, E. Hu, J. Xu, T. Deng, L. Ma, Y. Wang, X. Q. Yang and C. Wang, *J. Am. Chem. Soc.*, 2020, **142**, 21404-21409.

135 J. Ge, L. Fan, A. M. Rao, J. Zhou and B. Lu, *Nat. Sustain.*, 2021, DOI:10.1038/s41893-021-00810-7.

136 L. Shan, Y. Wang, S. Liang, B. Tang, Y. Yang, Z. Wang, B. Lu and J. Zhou, *InfoMat.*, 2021, **3**, 1028-1036.

137 M. Wang, C. W. Cao, F. Su, Y. Wang, W. Wang, C. Ding, J. R. Bai, T. Y. Liu, X. N. Sun and J. T. Zhang, *J. Power Sources*, 2020, **477**, 229013.

138 X. Dong, J. Sun, Y. Mu, Y. Yu, T. Hu, C. Miao, C. Huang, C. Meng and Y. Zhang, *J. Colloid Interface Sci.*, 2022, **610**, 805-817.

139 J. Guo, W. Ma, Z. Sang, X. Zhang, J. Liang, F. Hou, W. Si, S. Wang and D. Yang, *Chem. Eng. J.*, 2022, **428**, 132644.

140 D. Aurbach, Z. Lu, A. Schechter, Y. Gofer, H. Gizbar, R. Turgeman, Y. Cohen, M. Moshkovich and E. Levi, *Nature*, 2000, **407**, 724-727.

141 A. D. Tevar, M. D. Graef and J. Whitacre, J. *Meet. Abstr.*, 2008, **MA2008-02**, 642.

142 S. I. Park, I. Gocheva, S. Okada and J. Yamaki, *J. Electrochem. Soc.*, 2011, **158**, A1067.

143 C. D. Wessells, S. V. Peddada, R. A. Huggins and Y. Cui, *Nano Lett.*, 2011, **11**, 5421-5425.

144 S. Liu, J. J. Hu, N. F. Yan, G. L. Pan, G. R. Li and X. P. Gao, *Energy Environ. Sci.*, 2012, **5**, 9743-9746.

145 Y. Mizuno, M. Okubo, E. Hosono, T. Kudo, K. Oh-ishi, A. Okazawa, N. Kojima, R. Kurono, S. Nishimura and A Yamada, *J. Mater. Chem. A*, 2013, **1**, 13055-13059.

146 J. Zheng, Q. Zhao, T. Tang, J. Yin, C. D. Quilty, G. D. Renderos, X. Liu, Y. Deng, L. Wang, D. C. Bock, C. Jaye, D. Zhang, E. S. Takeuchi, K. J. Takeuchi, A. C. Marschilok and L. Archer, *Science*, 2019, **366**, 645-648.